



Ultrastructural and molecular characterization of *Vairimorpha austropotamobii* sp. nov. (Microsporidia: Burenellidae) and *Thelohania contejeani* (Microsporidia: Thelohaniidae), two parasites of the white-clawed crayfish, *Austropotamobius pallipes* complex (Decapoda: Astacidae)



Tobia Pretto^{a,b,*}, Francesco Montesi^c, Daniela Ghia^d, Valeria Berton^c, Miriam Abbadi^c, Michele Gastaldelli^a, Amedeo Manfrin^a, Gianluca Fea^d

^a National Reference Centre for Crustacean Diseases, Istituto Zooprofilattico Sperimentale delle Venezie, Via Leonardo da Vinci 39, 45011 Adria, Rovigo, Italy

^b Department of Veterinary Medical Sciences, Alma Mater Studiorum University of Bologna, Via Tolara di Sopra 50, 40064 Ozzano dell'Emilia, Bologna, Italy

^c Department of Comparative Biomedical Sciences, Istituto Zooprofilattico Sperimentale delle Venezie, Viale dell'Università 10, 35020 Legnaro, Padova, Italy

^d Department of Earth and Environmental Sciences, University of Pavia, Via Adolfo Ferrata 7, I-27100 Pavia, Italy

ARTICLE INFO

Keywords:
Vairimorpha austropotamobii sp. nov.
Thelohania contejeani
Austropotamobius pallipes complex
Microsporidia
SSU rRNA
RPB1

ABSTRACT

The microsporidiosis of the endangered white-clawed crayfish *Austropotamobius pallipes* complex has generally been attributed to only one species, *Thelohania contejeani*, the agent of porcelain disease. Species identification was mostly assessed by macroscopic examination or microscopic evaluation of muscle samples rather than by molecular or ultrastructural analyses. A survey conducted on *A. pallipes* complex populations in Northern Italy highlighted the presence of two different microsporidia causing similar muscular lesions, *T. contejeani* and an undescribed octosporoblastic species *Vairimorpha austropotamobii* sp. nov. Mature spores and earlier developmental stages of *V. austropotamobii* sp. nov. were found within striated muscle cells of the thorax, abdomen, and appendages of the crayfish. Only octosporoblastic sporogony within sporophorous vesicles (SPVs) was observed. Diplokaryotic sporonts separated into two uninucleate daughter cells, which gave rise to a rosette-shaped plasmodium, and eight uninucleate spores were produced within the persistent SPV. Ultrastructural features of stages in the octosporoblastic sequence were similar to those described for *Vairimorpha necatrix*, the type species. Mature spores were pyriform in shape and an average of 3.9 × 2.2 μm in size. The polar filament was coiled 11–14 times, lateral to the posterior vacuole. The small subunit ribosomal RNA gene (SSU rRNA) and the large subunit RNA polymerase II gene (RPB1) of *V. austropotamobii* sp. nov. were sequenced and compared with other microsporidia. The highest sequence identity of SSU rRNA (99%) and RPB1 (74%) genes was with the amphipod parasite *Nosema granulosis* and subsequently with *V. cheracis*, which infects the Australian yabby *Cherax destructor*. In our work we discuss about the reasons for placing this new species in the genus *Vairimorpha*. In addition, we provide for *T. contejeani* a RPB1 gene sequence, supplemental sequences of SSU rRNA gene and ultrastructural details of its sporogony in the host *A. pallipes* complex.

1. Introduction

Microsporidia are intracellular eukaryotic parasites infecting almost all invertebrate phyla. The majority of species are described from arthropods, particularly insects and crustaceans (Wittner and Weiss, 1999). Fifty genera within the Microsporidia infect four major classes of crustacean hosts: Malacostraca, Maxillipoda, Ostracoda and Branchiopoda (Stentiford et al., 2013). Four microsporidian genera (*Thelohania*, *Vairimorpha*, *Pleistophora*, *Vavraia*) have been described infecting

freshwater crayfish of the superfamily Astacoidea (Longshaw, 2011). In the genus *Thelohania* (Henneguy and Thelohan, 1892) three species (*Thelohania contejeani*, *T. parastaci*, *T. montirivulorum*) were described in detail, through ultrastructural and molecular data in European and Australian crayfish (Lom et al., 2001; Moodie et al., 2003a, 2003b). Other microsporidia assigned to the genus *Thelohania*, as *T. cambari* parasite of *Cambarus bartonii* (Sprague, 1950), have been reported in *Cambarellus shufeldti* (Sogandares-Bernal, 1962), *Paranephrops planifrons* (Jones, 1980) and *Cherax quadricarinatus* (Herbert, 1988) but were

* Corresponding author at: National Reference Centre for Crustacean Diseases, Istituto Zooprofilattico Sperimentale delle Venezie, Via Leonardo da Vinci 39, 45011 Adria, Rovigo, Italy.

E-mail address: tpretto@izsvenezie.it (T. Pretto).

incompletely characterized. *Thelohania* species in crayfish proliferate within the musculature, with infected animals showing whitish or opaque abdomen giving rise to the common name of porcelain disease or “cotton tail”. This chronic infection causes progressive impairment of the locomotor apparatus and cardiac function and eventually results in the death of the host. *T. contejeani* developmental stages and mature spores were observed not only in the abdominal and limb muscles but also in (i) the myocardium, (ii) the musculature of the eyestalk, (iii) the longitudinal muscles of the hind gut and cardiac stomach (Cossins and Bowler, 1974). Other infected tissues were the nervous system, such as the supra-oesophageal ganglion (Cossins and Bowler, 1974) and the ventral nerve chord, the connective tissue of the ovary (Vey and Vago, 1973; Oidtmann, 1996) and the haemolymph with spores either free (Cossins and Bowler, 1974) or inside fixed haemocytes in the gills (Quaglio et al., 2011). *T. contejeani* infects members of the family Astacidae (*Astacus astacus*, *A. leptodactylus*, *Austropotamobius pallipes* complex and *Pacifastacus leniusculus*) and Cambaridae (*Orconectes (Faxonius) limosus*) in Europe (Edgerton et al., 2002; Dunn et al., 2009). Putative *T. contejeani* infections in *Orconectes virilis* (France and Graham, 1985) and *O. limosus* in North America (McGriff and Modin, 1983), and of *Paranephrops zealandicus* (Quilter, 1976) in New Zealand were described; however, identification was based on spore size as molecular/ultrastructural confirmation was lacking in these studies. *T. contejeani* presents a dimorphic pattern of sporogony (Lom et al., 2001), with simultaneous presence of diplokaryotic sporonts producing uninucleate spores with 9–10 turns of the polar filament within a sporophorous vesicle (SPV), and single diplokaryotic sporonts producing diplokaryotic spores with 5–6 turns of the polar filament in small membrane-bound compartments. Similar dimorphic sporogony with binucleate and uninucleate mature spores inside a SPV was observed in the species *T. parastaci* and *T. montirivulorum*, parasites of the Australian yabby *Cherax destructor*, collected from lowland and highland populations, respectively. Both species mainly target the skeletal muscles (abdomen, pereiopods, chelipeds and thorax) and those associated with the digestive tract and the heart; *T. parastaci* developmental stages were observed also in the haemocytes of the hepatopancreas and in the haemolymph of the gill filaments. A third octosporoblastic microsporidian parasite, *Vairimorpha cheracis*, was described in highland populations of *C. destructor* (Moodie et al., 2003c), co-infected by *T. montirivulorum*. *V. cheracis* has a putative monomorphic sporogony, characterized by pyriform uninucleate mature spores ($3.4 \times 1.9 \mu\text{m}$) with 10–12 turns of the polar filament contained inside a SPV. It mainly affects the crayfish skeletal muscle of the abdomen, thorax and appendages and mature SPVs are present in low numbers also in the intestinal submucosa and between follicular cells of the ovary. This species has been ascribed to the genus *Vairimorpha* due to similarities with the type species *V. necatrix* in ultrastructural characteristics and phylogeny based on small subunit ribosomal RNA (SSU rRNA) gene sequences (Moodie et al., 2003c). SSU rRNA gene is the most common target for molecular confirmation of microsporidian infections and has been extensively applied for taxonomic purpose to supplement data gathered by classical methods, based on spore morphology, developmental sequences and life cycles characteristics. The SSU rRNA gene has been widely used because of the juxtaposition of conserved and non-conserved regions of DNA along its length (McManus and Bowles, 1996), although it is considered the most slowly evolving of the rDNA sequences (Hillis and Dixon, 1991) and is substantially shorter than both other fungi and most prokaryotes, rarely permitting to unambiguously assign a topology to trees comparing closely related species (Ironside, 2007). In order to improve the detail of distinction between close related species, phylogenetic analyses based on the largest sub-unit of the RNA polymerase II gene (RPB1), which is a faster-evolving target (Cheney et al., 2001), have been increasingly investigated especially in the genera *Nosema*/*Vairimorpha* (Ironside, 2007). Porcelain disease in the Italian populations of white-clawed crayfish has been observed only in three northern regions: Liguria (Mori

and Salvidio, 2000), Veneto (Quaglio et al., 2011) and Trentino (Endrizzi et al., 2013). The microsporidian infections described in these works referred to the species *Thelohania contejeani* based on morphological and ultrastructural evaluations without a molecular confirmation. In this study we applied both the ultrastructural observation and molecular analyses to identify the microsporidian parasites of *A. pallipes* complex specimens collected from streams in Northern and Central Italy and to confirm the presence of *T. contejeani*.

2. Material and methods

2.1. Sources of infected hosts

A. pallipes complex adult specimens of both sexes belonging to three subspecies; *A. italicus carsicus*, *A. i. carinthiacus* and *A. i. meridionalis* following the classification proposed by Fratini et al. (2005), were sampled. Specimens suspected of microsporidiosis due to whitening of the abdominal flexor muscle, were collected by hand from small streams and headwaters in Northern and Central Italy. The sampling locations; 3 creeks from the Po river catchment (Lombardy region) and one stream from Abruzzo region are described in Table 1. All crayfish were submitted to the laboratory alive.

2.2. Macroscopic observation and sampling

The abdominal musculature was evaluated and changes from the normal grayish-translucent color of the pleon to a more whitish or yellowish and opaque appearance were recorded. The specimens were anesthetized on crushed ice before sectioning the cephalothorax through the cephalic ganglion. Samples of abdominal musculature were stored in EtOH 80% for molecular analysis. The cephalothorax and the abdomen were injected and fixed in Davidson's fixative for 48 h and post-fixed in EtOH 70%. Samples of abdominal muscle ($< 1 \text{ mm}^3$) were fixed in a solution of glutaraldehyde 2.5% and formaldehyde 2.5% in sodium cacodylate buffer and stored at + 4 °C for transmission electron microscopy analysis.

2.3. Cytology (light microscopy)

Muscle imprints and fresh squashes preparations were obtained from the abdominal muscle or chelipeds of macroscopically affected specimens in order to confirm the microsporidian infection. Fresh preparations of muscle tissue in 0.9% NaCl saline were examined at 1000 magnification under a Leitz Diaplan light microscope (Leica, UK). Impression smears of the affected muscle were air-dried, and either directly observed or further fixed in methanol and stained with haematological staining (Hemacolor®, Merk) or 10% Giemsa and mounted in Eukitt® resin. Digital images and measurements were obtained using an integrated LEICA MC170HD (Leica, UK) camera and LAS 4.5.0 (Leica, UK) software.

2.4. Histology

Fixed samples were further reduced in size and for each specimen longitudinal and transversal sections of the abdomen and a longitudinal section of the cephalothorax, including the cardial stomach, hepatopancreas, gonads, green gland, ventral nerve chord, heart and gills were obtained. Tissues were dehydrated and embedded in Paraplast® applying standard histological protocols. 3 μm thin sections were stained alternatively with Harris's haematoxiline and eosine-floxine or Giemsa stain, mounted in Eukitt® resin and observed with a Leitz Diaplan microscope at 40–1000 magnifications.

2.5. Transmission electron microscopy

Five specimens collected from the Po river catchment (Vincerino

Table 1
Sampling detail of microsporidian species infecting adult *A. pallipes* complex, with indication from which sample were obtained the sequences of SSU rRNA and RPB1 genes.

Location (river basin) [latitude, longitude] region	<i>Austropotamobius pallipes</i> complex subspecies		Sampling date	No. of crayfish host (gender)	Microsporidian species	Accession No. SSU rRNA sequence	Accession No. RPB1 sequence
Agna stream (Oglio-Po) [45°41'–10°30'] Lombardy	<i>Austropotamobius italicus carsicus</i> ^a		September 2011 September 2012 October 2013	3 (♂) 4 (2♀; 2♂) 1 (♀)	<i>Thelobiania contejeani</i> <i>Vairimorpha austropotamobii</i> sp. nov and <i>Thelobiania contejeani</i> <i>Thelobiania contejeani</i>	MF344630, MF344633	MF344628
Foce stream (Lambro-Po) [45°51'–09°16'] Lombardy	<i>Austropotamobius italicus carinthiacus</i> ^a						
Fino stream (Tirino) [42°28'–13°46'] Abruzzo Vincenzo stream (Mincio-Po) [45°42'–10°37'] Lombardy	<i>Austropotamobius italicus meridionalis</i> ^b <i>Austropotamobius italicus carsicus</i> ^a		September 2013 September 2012 September 2014 October 2015	2 (1♀; 1♂) 3 (2♀; 1♂) 2 (1♀; 1♂) 13 (8♀; 5♂)	<i>Thelobiania contejeani</i> <i>Vairimorpha austropotamobii</i> sp. nov. <i>Vairimorpha austropotamobii</i> sp. nov. <i>Vairimorpha austropotamobii</i> sp. nov.	MF344634, MF344635	MF344629

^a Bernini et al. (2016).
^b Jelić et al. (2016).

and Agna streams), identified as *V. austropotamobii* sp. nov. by molecular analyses, and three *T. contejeani* positive specimens from Agna, Foce and Fino streams were ultrastructurally examined. Samples of fixed abdominal muscle were washed three times in fresh 0.1 M cacodylate buffer and postfixed for 2 h in 1% osmium tetroxide. Fixed samples were dehydrated through a graded acetone series (30%–50%–70%–90%–100%). Each sample was embedded into Durcupan ACM resin after initial infiltration of the resin using a resin-acetone dilution series (20% for 1 h; 30% and 50% for 1 h and 30 min; 75% overnight). Polymerization was activated by heating the resin to 40 °C for 24 h and 60 °C for 48 h. Blocks were cut into ultra-thin sections using an ultramicrotome Ultracut Richter Young, equipped with diamond blade (DiATOME), and stained using uranyl acetate and Reynolds lead citrate prior to examination with a Philips EM208S transmission electron microscope operated at 80 kV. Micrographs were recorded on a side mounted MegaView 3 camera and the image analysis was performed using the analytical imaging software “iTEM” (Olympus, Münster Germany).

2.6. Amplification and cloning of SSU rDNA

From each specimen, 25–30 mg of abdominal muscle were taken for total genomic DNA extraction using QIAamp DNA Mini Kit (QIAGEN), according to the manufacturer's instructions (tissue protocol). The DNA sample were eluted in a buffer supplied by Qiagen, quantified through spectrophotometer (BioPhotometer – Eppendorf) and stored at –80 °C for long-term preservation. The detection of the microsporidian DNA in suspected samples was based on the work by Imhoff et al. (2010). The generic microsporidian primers V1f-1492r (Weiss et al., 1994) were used to amplify a portion (~1360 bp) of the small subunit ribosomal RNA gene (SSU rDNA). Other generic microsporidian primers 18sf-350sr (Baker et al., 1995) or *T. contejeani* species-specific primers MIC5-1 and MIC3-4 (Imhoff et al., 2010) were applied for confirmation or when unexpected negative amplification were obtained with V1f-1492r primers. Details of the PCR protocols are provided in Table 2. PCR products were analyzed by electrophoresis in 1.5% agarose gel (Sigma-Aldrich, St. Louis, MO) after staining with 0.1 µl/ml GelRedTM Nucleic Acid Gel Stain (Biotium, Hayward, CA). A PCR using the Platinum® Taq DNA Polymerase (Invitrogen, Carlsbad, CA, USA) and the V1f-1492r primers was performed on two samples positive for the two different microsporidia (*T. contejeani* and *V. austropotamobii* sp. nov.). Amplicons with the correct size were subsequently purified through the QIAquick gel extraction Kit (Qiagen) and cloned into a TA cloning® vector (Invitrogen) as described by the manufacturer. For both microsporidia, different clones were chosen and the sequence of the DNA inserts was verified by sequencing using specific vector primers and V1f-1492 r primers.

2.7. Amplification of RPB1 gene

For the amplification of RPB1 in confirmed positive samples of *T. contejeani* and *V. austropotamobii* sp. nov., a degenerated primer set (RPB1011f: 5'-GARATGAAYCTNCAYATGCC-3'; RPB2041r: 5'-CCCATRGCRTGRAARWARAA-3') was designed on conserved regions of the gene, identified in a group of different *Nosema*/Vairimorpha species following the work by Ironside (2007). The obtained amplicon spanned about 1000 bp. Details of the PCR protocol are provided in Table 2.

2.8. Sequencing and phylogenetic analysis

PCR products were purified with ExoSAP-IT® (USB Corporation, Cleveland, OH) and sequenced in both directions using the Big Dye Terminator v3.1 cycle sequencing kit (Applied Biosystems, Foster City, CA). Sequencing reactions were cleaned-up using the CENTRI-SEP 96 Well Plates (Princeton Separations, Inc.) and analyzed on a 16-capillary ABI PRISM 3130xl Genetic Analyzer (Applied Biosystems, Foster City,

Table 2

PCR protocols: primers, expected fragment size, reagents and PCR thermal cycles for each reaction.

	SSU rDNA			RPB1
	Generic	Generic	<i>Thelohania</i> -specific	
Primers	V1f-1492r ^a	18sf-350sr ^b	MIC5-1-MIC3-4 ^c	RPB1011f-RPB2041r ^d
Expected fragment (bp)	~1360	~310	~215	~1000
<i>Reagents</i>				
Molecular graded H2O (μl)	14.425	18.425	18.175	14.425
10× PCR Rxn Buffer (μl)	2.5	2.5	2.5	2.5
MgCl2 50 mM (mM)	2	2	2	2
dNTPs (mM)	0.8	0.8	0.8	0.8
F primer (μM)	0.4	0.4	0.4	0.4
R primer (μM)	0.4	0.4	0.4	0.4
Platinum Taq (U)	0.625	0.625	0.625	0.625
DNA (μl)	5	1	1	5
<i>PCR</i>				
Initial denaturation	94 °C; 2 min	94 °C; 2 min	94 °C; 2 min	94 °C; 2 min
Cycles (40)	94 °C; 1 min 51 °C; 1 min 72 °C; 2 min	94 °C; 30 s 51 °C; 1 min 72 °C; 30 s	94 °C; 30 s 51 °C; 30 s 72 °C; 30 s	94 °C; 1 min 51 °C; 1 min 72 °C; 2 min
Final extension	72 °C; 10 min	72 °C; 5 min	72 °C; 5 min	72 °C; 10 min

^a V1f: 5'-CACCAGGTTGATTCTGCCGTGAC-3'; 1492r: 5'-GGTACCTTGACTT-3'.^b 18sf: 5'-GTGATTCTGCCGTGACGT-3'; 350sr: 5'-TTCCGGCCCTGCTGCCGTCTTGG-3'.^c MIC5-1: 5'-ATAACAGGTCACTGATGCCCT-3'; MIC3-4: 5'-ACCCTAATATCCATCTGAGA-3'.^d RPB1011f: 5'-GARATGAAYCTNCAYATGCC-3'; RPB2041r: 5'-CCCATRGCRTGRAARWARAA-3'.

CA, USA). Sequencing data were assembled and edited using dedicated softwares as Sequencing Analysis 5.2 and SeqScape v2.5 (Applied Biosystems). The sequences obtained of SSU rDNA were aligned using the MEGA 5 software (Tamura et al., 2011) and compared to reference sequences available in GenBank of SSU rDNA from 50 microsporidia representative of genera infecting aquatic organisms (Table 3), according to Vossbrinck and Debrunner-Vossbrinck (2005). Two species were chosen as outgroup, *Heterococcus pleurococcooides* and *Conidiobolus coronatus*. Besides, RPB1 sequences of *V. austropotamobii* sp. nov. and *T. contejeani* were aligned, using the software, with other microsporidia (Table 4) of the Class Terresporidia (Ironside, 2007), Aquasporidia and Marinospordia (Cheney et al., 2001). In order to identify the best nucleotide-substitution model describing the phylogenetical relationships among the aligned sequences, MEGA 5 model selection function was employed. The goodness-of-fit to the data was evaluated by the Bayesian information criterion (BIC) score, which showed general time reversible (GTR) model with gamma-distributed among-site rate variation (with four rate categories, Γ4) as the best performing with both datasets. Maximum-likelihood trees were then constructed with the software PhyML v3.1 (Guindon et al., 2010) via a SPR branch-swapping search procedure (Darriba et al., 2012). To assess the robustness of individual nodes, 1000 bootstrap replicates were performed using the same substitution model previously identified. Phylogenetic trees were finally visualized with the software FigTree v1.4 (<http://tree.bio.ed.ac.uk/software/figtree/>).

3. Results

3.1. Macroscopic observation

All suspected crayfish sampled in the field showed various degrees of infection in the musculature, from a light opalescence to a generalized whitish appearance of the ventral abdomen and chelipeds. A reduction of mobility and tail flick response was observed in the most severe cases. Specimens of both genders sampled in two streams of the Po river catchment (Agna and Vincenzo streams), parasitized by *V. austropotamobii* sp. nov., showed distinctive affected fibers scattered between normal muscle tissue in cases of moderate infection (Fig. 1B), while in advanced infection the pleonal musculature progressed to homogenous yellowish-cream white discoloration (Fig. 1A). Necropsy

showed that the pleonal extensor and flexor muscles, the mandibular and longitudinal musculature of the cephalothorax and the levator and depressor muscles of the pereiopods and chelipeds (opener–closer muscle of the claw) had been affected. Specimens of both genders parasitized by *T. contejeani* (Fig. 2A) showed a more chalk-white discoloration of the ventral abdomen and chelipeds, and in highly affected specimens the cardiac musculature presented whitish streaks.

3.2. Cytology

Muscle imprints showed the presence of microsporidian spores in all the macroscopically affected samples. The spores at different levels of development (sporoblasts-mature spores) were either free or contained in sporophorous vesicles of parasitic origin with a constant number of eight spores in each vesicle. The proportion between free spores and spores inside the sporophorous vesicles was substantially different between specimens parasitized by *T. contejeani* and *V. austropotamobii* sp. nov. Crayfish affected by *V. austropotamobii* sp. nov. showed imprints with predominance of spores contained inside a SPV (Fig. 1C and D). The sporophorous vesicles were spherical in shape, with a diameter of $7.9 \pm 0.4 \mu\text{m}$ ($n = 50$). Spores inside a SPV presented an oval-pyriform shape and measured $3.9 \pm 0.4 \mu\text{m} \times 2.2 \pm 0.3 \mu\text{m}$ ($n = 50$). Single mature spores released from broken SPVs were pyriform. In *T. contejeani* infected specimens the majority of mature spores were free and not contained inside a SPV (Fig. 2B). They appeared binucleated in Giemsa staining, ovoid with wide posterior end and their size ranged $3.3 \pm 0.45 \mu\text{m} \times 1.7 \pm 0.2 \mu\text{m}$ ($n = 50$). The sporophorous vesicles were roughly spherical in shape, with a diameter of $9.4 \pm 0.6 \mu\text{m}$ ($n = 20$). The spores inside the SPVs presented an oval shape, were uninucleated and slightly large, $3.6 \pm 0.4 \mu\text{m} \times 2.3 \pm 0.3 \mu\text{m}$ ($n = 50$).

3.3. Histology

Affected specimens showed proliferation of microsporidia at different developmental stages inside the skeletal musculature, with substitution of normal muscle fibrils with free spores and sporophorous vesicles. The striated muscle fibers presented normal peripheral nuclei and intact sarcolemma (Fig. 1E–G) with evidence of binucleated cells with amphophilic cytoplasm referable to the meront/sporont stage of

Table 3

Microsporidian and two outgroup SSU rRNA gene sequences used in phylogenetic analysis.

Microsporidia	Host	Accession No.	Class ^a
<i>Cystosporogenes operophterae</i>	<i>Operophtera brumata</i> (I)	AJ278949	Terresporidia
<i>Encephalitozoon cuniculi</i>	<i>Homo sapiens</i> (M)	L39107	Terresporidia
<i>Enterocytozoon bieneusi</i>	<i>Homo sapiens</i> (M)	L07123	Terresporidia
<i>Enterocytozoon hepatopenaei</i>	<i>Penaeus monodon</i> (C)	KF362130	Terresporidia ^d
<i>Nosema apis</i>	<i>Apis mellifera</i> (I)	X73894	Terresporidia
<i>Nosema bombyi</i>	<i>Bombus terrestris</i> (I)	AY008373	Terresporidia
<i>Nosema bombycis</i>	<i>Bombyx mori</i> (I)	D85504	Terresporidia
<i>Nosema ceranae</i>	<i>Apis cerana</i> (I)	U26533	Terresporidia
<i>Nosema dissitiae</i>	<i>Malacosoma dissitiae</i> (I)	HQ457438	Terresporidia
<i>Nosema fumiferanae</i>	<i>Epiphys postvittana</i> (I)	HQ457435	Terresporidia
<i>Nosema furnacalis</i>	<i>Ostrinia furnacalis</i> (I)	U26532	Terresporidia
<i>Nosema granulosis</i>	<i>Gammarus duebeni</i> (C)	AJ011833	Terresporidia
<i>Nosema oulmae</i>	<i>Oulema melanopus</i> (I)	U27359	Terresporidia
<i>Nosema pyrausta</i>	<i>Ostrinia nubilalis</i> (I)	AY958071	Terresporidia
<i>Nosema trichoplusiae</i>	<i>Apis cerana</i> (I)	U09282	Terresporidia
<i>Nosema tyriae</i>	<i>Tyria jacobaeae</i> (I)	AJ012606	Terresporidia
<i>Vairimorpha austropotamobii</i> sp. nov. clone 1	<i>Austropotamobius pallipes</i> complex (C)	MF344634	Terresporidia ^b
<i>Vairimorpha austropotamobii</i> sp. nov. clone 2	<i>Austropotamobius pallipes</i> complex (C)	MF344635	Terresporidia ^b
<i>Vairimorpha cheracis</i>	<i>Cherax destructor</i> (C)	AF327408	Terresporidia
<i>Vairimorpha disparis</i>	<i>Lymantria dispar</i> (I)	JX239748	Terresporidia
<i>Vairimorpha imperfecta</i>	<i>Plutella xylostella</i> (I)	AJ131645	Terresporidia
<i>Vairimorpha lymantriae</i>	<i>Lymantria dispar</i> (I)	AF033315	Terresporidia
<i>Vairimorpha necatrix</i>	<i>Pseudaletia unipuncta</i> (I)	Y00266.1	Terresporidia
<i>Vittaforma cornae</i>	<i>Homo sapiens</i> (M)	JX123133	Terresporidia
<i>Ameson michaelis</i>	<i>Callinectes sapidus</i> (C)	L15741	Marinosporidia
<i>Dictyocoela duebenum</i>	<i>Gammarus duebeni</i> (C)	KP091740	Marinosporidia
<i>Dictyocoela muelleri</i>	<i>Gammarus duebeni celticus</i> (C)	AJ438955	Marinosporidia
<i>Glugea americanus</i>	<i>Lophius americanus</i> (F)	AF056014	Marinosporidia
<i>Glugea hertwigi</i>	<i>Osmerus</i> sp. (F)	GQ203287	Marinosporidia
<i>Kabatana takedai</i>	<i>Oncorhynchus</i> sp. (F)	AF356222	Marinosporidia
<i>Loma acerinae</i>	<i>Myrophis platyrrhynchus</i> (F)	AJ252951	Marinosporidia
<i>Microgemma caulleryi</i>	<i>Hyperoplus lanceolatus</i> (F)	AY033054	Marinosporidia
<i>Myosporidium merluccius</i>	<i>Merluccius</i> sp. (F)	AY530532	Marinosporidia
<i>Nadelspora canceri</i>	<i>Carcinus maenas</i> (C)	AY958070	Marinosporidia
<i>Pleistophora mulleri</i>	<i>Gammarus duebeni celticus</i> (C)	EF119338	Marinosporidia
<i>Potaspora aequidens</i>	<i>Aequidens plagiozonatus</i> (F)	KP404613	Marinosporidia
<i>Spraguea lophii</i>	<i>Lophius piscatorius</i> (F)	AF104086	Marinosporidia
<i>Tetramicra brevifilum</i>	<i>Scophthalmus maximus</i> (F)	AF364303	Marinosporidia
<i>Thelohania butleri</i>	<i>Pandalus jordani</i> (C)	DQ417114	Marinosporidia ^e
<i>Triwangia caridinae</i>	<i>Caridina formosae</i> (C)	JQ268567	Marinosporidia ^c
<i>Vavraia culicis</i>	<i>Culicidae</i> (I)	AJ278956	Marinosporidia
<i>Amblyospora cinerei</i>	<i>Aedes cinereus</i> (I)	AY090057	Aquasporidia
<i>Paranosema (Antonospora) locustae</i>	<i>Acrididae</i> (I)	AY305324	Aquasporidia
<i>Antonospora scoticae</i>	<i>Andrena scotica</i> (I)	AF024655	Aquasporidia
<i>Edhazardia aedis</i>	<i>Aedes aegypti</i> (I)	AF027684	Aquasporidia
<i>Kneallhazia solenopsae</i>	<i>Solenopsis invicta</i> (I)	AF031538	Aquasporidia
<i>Marssonella elegans</i>	<i>Cyclops vicinus</i> (C)	AY090041	Aquasporidia
<i>Parathelohania obesa</i>	<i>Anopheles quadrimaculatus</i> (I)	AY090065	Aquasporidia
<i>Visvesvaria algerae</i>	<i>Culicidae</i> (I)	AF024656	Aquasporidia
<i>Thelohania contejeani</i> TcC2	<i>Astacus fluviatilis</i> (C)	AF492593	Unresolved
<i>Thelohania contejeani</i> TcC3	<i>Astacus fluviatilis</i> (C)	AF492594	Unresolved
<i>Thelohania contejeani</i> clone 1	<i>Austropotamobius pallipes</i> complex (C)	MF344630	Unresolved ^b
<i>Thelohania contejeani</i> clone 2	<i>Austropotamobius pallipes</i> complex (C)	MF344633	Unresolved ^b
<i>Thelohania montirivulorum</i>	<i>Cherax destructor</i> (C)	AY183664	Unresolved
<i>Thelohania parastaci</i>	<i>Cherax destructor</i> (C)	AF294780	Unresolved
<i>Conidiobolus coronatus</i>	<i>Termitidae</i> (I), <i>Homo sapiens</i> (M)	AF296753	Out group
<i>Heterococcus pleurococcooides</i>	–	AJ579335	Out group

C: crustacea; F: fish; I: insect; M: mammal.

^a Following the classification proposed by Vossbrinck and Debrunner-Vossbrinck (2005).^b Discussed in our study.^c Wang et al. (2013).^d Tangprasitipap et al. (2013).^e Brown and Adamson (2006).

the parasite (Fig. 2C). In the center part of the fibers, sporogonic stages were evident (pansporoblasts, sporophorous vesicles with eight sporoblasts or eight mature spores, free spores). *T. contejeani* affected specimens, presented parasitized fibers with very high spore density, in the abdominal flexor muscle, thorax and pereiopods muscles, in the cardiac muscle (Fig. 2F) and longitudinal muscle fibers of the hind gut (Fig. 2G)

and the cardiac stomach. Another infected tissue was the ventral nerve chord (abdominal ganglia) where neuron bodies of the abdominal ganglia occasionally contained small spore masses (Fig. 2H and I). Crayfish infected by *V. austropotamobii* sp. nov. did not reveal any spores in the heart, and neither in the intestinal musculature (Fig. 1F) nor in the abdominal ganglia but only in the skeletal musculature of the

Table 4
Microsporidian RPB1 gene sequence used in phylogenetic analysis.

Microsporidia	Host	Accession No.	Class ^a
<i>Cystosporogenes operophterae</i>	<i>Operophtera brumata</i> (I)	AJ278949	Terresporidia
<i>Encephalitozoon cuniculi</i>	<i>Homo sapiens</i> (M)	NM001040904	Terresporidia
<i>Nosema apis</i>	<i>Apis mellifera</i> (I)	DQ996230	Terresporidia
<i>Nosema bombycis</i>	<i>Bombyx mori</i> (I)	DQ996231	Terresporidia
<i>Nosema disstriae</i>	<i>Malacosoma disstria</i> (I)	HQ457438	Terresporidia
<i>Nosema empoascaae</i>	<i>Empoasca fabae</i> (I)	DQ996232	Terresporidia
<i>Nosema fumiferanae</i>	<i>Epiphyas postvittana</i> (I)	HQ457435	Terresporidia
<i>Nosema granulosis</i>	<i>Gammarus duebeni</i> (C)	DQ996233	Terresporidia
<i>Nosema lymantiae</i>	<i>Lymantria dispar</i> (I)	JX213749	Terresporidia
<i>Nosema trichoplusiae</i>	<i>Apis cerana</i> (I)	DQ996234	Terresporidia
<i>Nosema tyrae</i>	<i>Tyria jacobaeae</i> (I)	AJ278948	Terresporidia
<i>Vairimorpha austropotamobi sp. nov.</i>	<i>Austropotamobius pallipes</i> complex (C)	MF344629	Terresporidia ^b
<i>Vairimorpha cheracis</i>	<i>Cherax destructor</i> (C)	DQ996235	Terresporidia
<i>Vairimorpha disparis</i>	<i>Lymantria dispar</i> (I)	JX239748	Terresporidia
<i>Vairimorpha necatrix</i>	<i>Pseudaletia unipuncta</i> (I)	DQ996236	Terresporidia
<i>Thelohania contejeani</i>	<i>Austropotamobius pallipes</i> complex (C)	MF344628	Unresolved ^b
<i>Vavraia culicis</i>	Culicidae (I)	AJ278956	Marinosporidia
<i>Glugea anomala</i>	<i>Gasterosteus aculeatus</i> (F)	AJ278952	Marinosporidia
<i>Loma acerinae</i>	<i>Myrophis platyrhynchus</i> (F)	AJ278951	Marinosporidia
<i>Pleistophora hippoglossoideoes</i>	<i>Hippoglossoides platessoides</i> (F)	AJ278950	Marinosporidia
<i>Pleistophora mulleri</i>	<i>Gammarus duebeni celticus</i> (C)	EF119338	Marinosporidia
<i>Paranosema (Antonospora) locustae</i>	Acrididae (I)	AF061288	Aquasporidia

C: crustacean; F: fish; I: insect; M: mammal.

^a Following the classification proposed by Vossbrinck and Debrunner-Vossbrinck (2005).

^b Discussed in our study.

thorax, abdomen, pereiopods and eyestalk (Fig. 1H). Moreover, an immune response was recorded against *T. contejeani* infected muscle fibers, characterized by haemocytic infiltrations (mostly hyalinocytes) inside and at the periphery of the fragmented fibers (Fig. 2D), with abundant melanin deposition (Fig. 2E). This response was constantly observed in every crayfish affected by *T. contejeani*, in a limited number of fibers per specimen, but was never detected in crayfish affected by *V. austropotamobii* sp. nov.

3.4. Transmission electron microscopy of *Vairimorpha austropotamobii* sp. nov.

3.4.1. Meronts

Meronts appeared as diplokaryotic cells ($4.6 \times 3.4 \mu\text{m}$; $n = 8$) delimited by a simple plasmalemma (Fig. 3B and C). Their cytoplasm contained scarce endoplasmic reticulum (ER) and ribosomes in comparison to sporonts. The two adhering nuclei were approximately $1.3 \mu\text{m}$ in diameter ($n = 8$) and presented one or two small nucleoli (Fig. 3B). Meronts were mostly in contact with the host cytoplasm and muscle fibrils (Fig. 3B).

3.4.2. Sporonts and sporoblasts

Sporonts appeared as larger cells ($5.9 \times 4.1 \mu\text{m}$; $n = 10$) with a distinctively thickened wall in comparison to the meront stage (Fig. 3A and D). Sporonts in our material appeared mostly binucleated

and were contained inside a sporophorous vesicle, which appears to originate as a layer of secretion generated by the pathogen through delamination from the sporontal plasmalemma, delimiting an episporontal space with aggregation of electron dense granular material (Fig. 3E). The sporont showed cytokinesis with separation of two daughter cells inside the SPV (Fig. 3E) and subsequent rosette-like segmentation, which gave rise to uninucleated sporoblasts. Up to four continuous lobes were observed in sections of sporogonial plasmodia (Fig. 3G and H). In comparison to *T. contejeani* no cylinders or coiled fibers were present adhering to the sporontal membrane (Fig. 3D and E). Moreover, tubular structures in the episporontal space were fewer in number and of a smaller size (Fig. 3K), with a diameter of 84 nm ($n = 10$). Maturing uninucleated sporoblasts of $3.2 \times 1.4 \mu\text{m}$ ($n = 8$) in size, were detected only inside the SPV and characterized by a distinct endoplasmic reticulum surrounded by a finely granular sporoplasm and a crescent-shaped electron dense polar capsule around the anchoring disc (Fig. 3J and K). The number of coils of the polar filament increased as sporoblast matured and the exospore layer thickened (40 nm $n = 8$). The shape of the sporoblasts changed from elongated to pyriform during the maturation process. At the posterior pole of the sporoblast an electron dense granular sporoplasm was evident between the posterior vacuole and the coils of the polar filament, which presented an electron-dense core (Fig. 3K).

3.4.3. Mature spores

In this study mature spores were present only inside the SPV (Fig. 3L) and were uninucleated (nuclear diameter 650 nm ; $n = 10$), with electron-dense anterior polaroplast and vesicular posterior polaroplast (Fig. 3M). There was no evidence of binucleated spores or presence of mature spores outside the membrane of the SPV in the samples analyzed. The endospore layer was formed at a late stage of spore maturation. The average thickness of the electron dense exospore and electron lucent endospore layers was 34 nm and 54 nm , respectively ($n = 10$); the endospore appeared thinner at the apex of the anchoring disc (27 nm ; $n = 4$) (Fig. 3O) and the outline of the exospores was crenelated (Fig. 3M–3N). The exospore wall appeared layered with a thin external electron dense layer, an electron lucent median layer and an inner thicker electron dense layer (Fig. 3O). The isofilar polar filament descended from the anchoring disc, with an initial diameter of 100 nm , through the polaroplast to the posterior pole of the spore, narrowing to a diameter of 74 nm ($n = 20$), where it coiled 11–14 times, lateral to the nucleus and the posterior vacuole (Fig. 3N).

3.5. Transmission electron microscopy of *Thelohania contejeani*

In the heavily infected muscle tissue, groups of sporonts were interspersed between clusters of free mature spores and maturing sporoblasts inside SPVs. Meronts were rather rare and were mostly found at the periphery of the affected fiber, close to the host sarcoplasma and muscle fibrils. As described by Lom et al. (2001) mature spores were observed either uninucleated and contained inside a SPV or binucleated and free. Although the final stages of the two route of sporogony were evident, the detailed sporogonial development producing diplokaryotic mature spores described in the above-mentioned study was not clearly identifiable in our samples.

3.5.1. Meronts

Meronts appeared as large diplokaryotic cells ($5.2 \times 3.8 \mu\text{m}$ ($n = 8$)), delimited by a simple plasma membrane (Fig. 4A). Their cytoplasm contained scarce endoplasmic reticulum (ER) and appeared vacuolated and more electron-lucent than the sporont stage. The nuclei were approximately $1.8 \mu\text{m}$ in diameter ($n = 10$) and presented one to three small nucleoli. It was not possible to differentiate the meronts giving rise to the two route of sporogony.

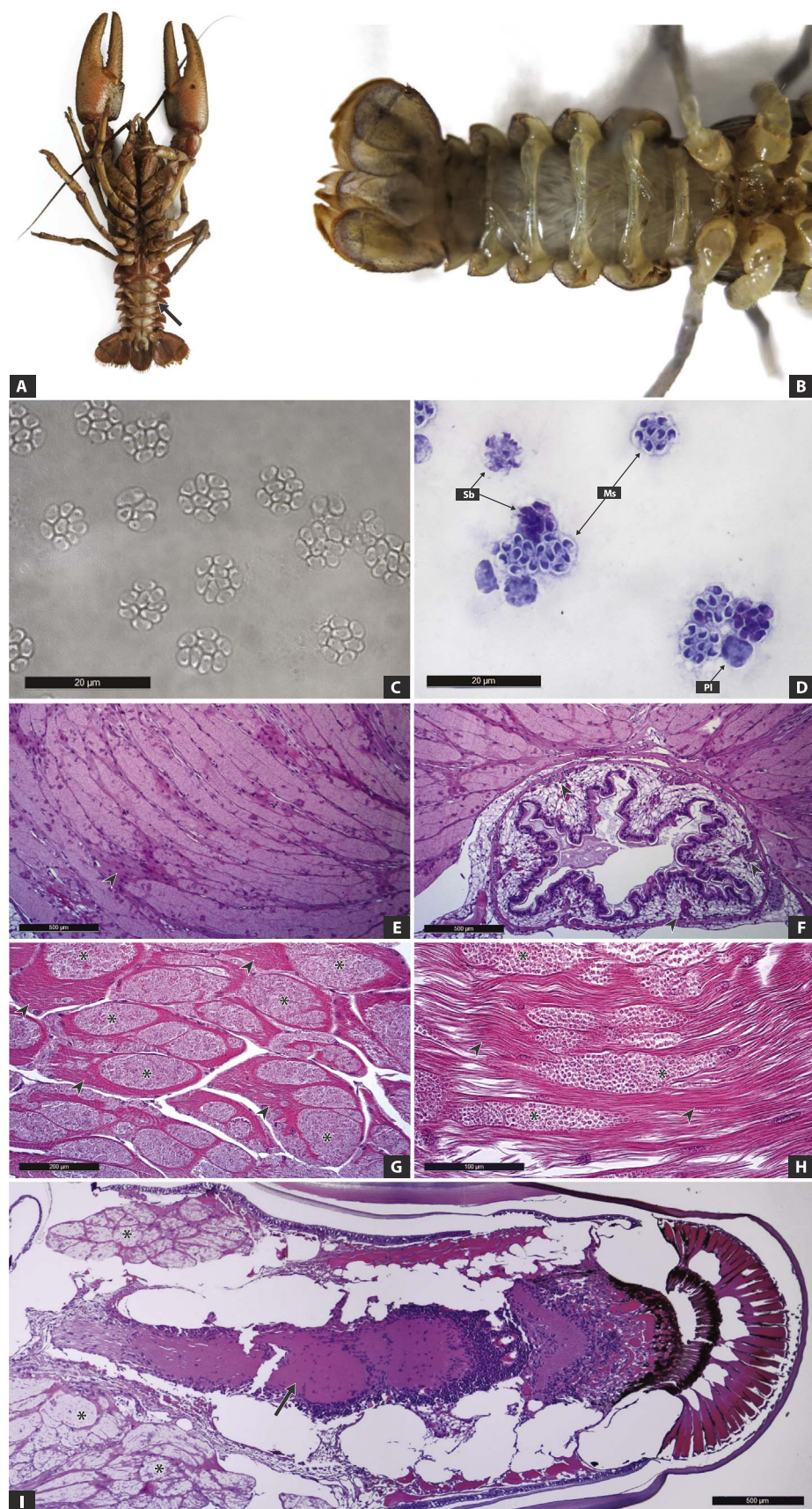
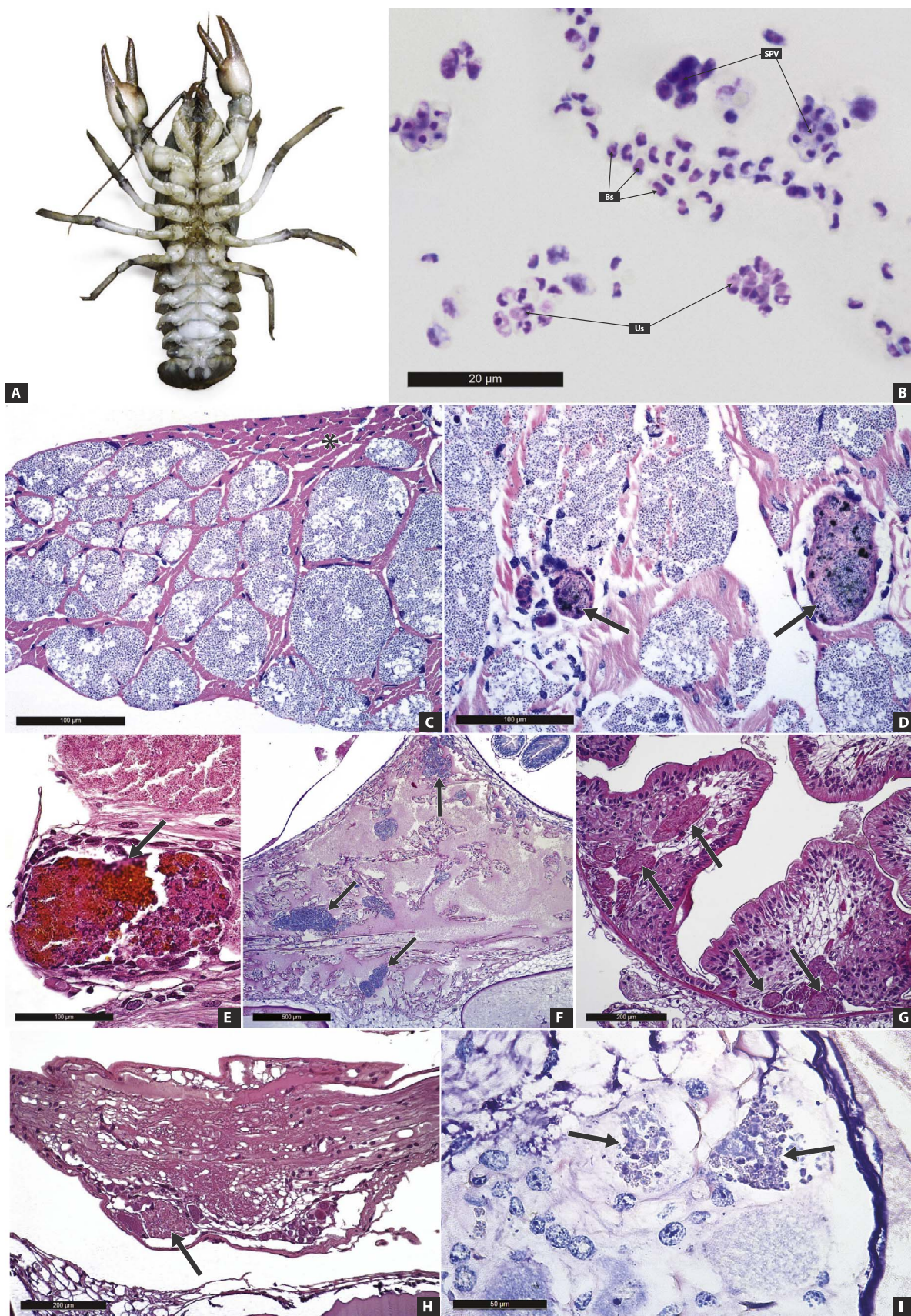


Fig. 1. Macroscopic and microscopic observation of *Vairimorpha austropotamobii* sp. nov. affected specimens: A: *Austropotamobius pallipes* complex severely affected by *Vairimorpha austropotamobii* sp. nov. Creamy white opaque appearance of the abdominal musculature (arrow). B: *A. pallipes* complex moderately affected. Parasitized whitish muscle fibers appear scattered among greyish unaffected ones. C: Light microscopy of unstained muscle imprint of *V. austropotamobii* sp. nov., 100×. Sporoporous vesicles (SPVs), each with eight pyriform spores. D: Light microscopy of Hemacolor®-stained muscle imprint, 100×. SPV with multinucleated plasmodia (Pl), SPV with maturing sporoblasts (Sb) and SPVs with mature spores (Ms). E: Histological appearance of *V. austropotamobii* sp. nov. affected skeletal muscle fibers of the pleon. The myofibres are replete by maturing stages of the microsporidia, while the sarcolemma is intact and there is no associated inflammatory response. Normal muscle fiber (arrowhead). H-E, 4×. F: Histological transverse section of the abdomen with evidence of the intestinal structure. The muscle fibers that constitute the muscular lamina of the gut (arrowheads) are not affected by *V. austropotamobii* sp. nov. H-E, 4×. G: Increased magnifications of the affected myofibers (*), and normal appearance of myofibres (arrowheads). H: In severely affected specimens the most prevalent developmental stage of the microsporidia is the maturing SPV. SPVs are clearly identifiable as discrete spherical bodies inside the myofibres (*). H-E, 10–25×. I: Longitudinal section of the eye-stalk. The retina and optic nerve (arrow) are not affected, while the associated skeletal musculature is strongly parasitized (*). H-E, 4×.



(caption on next page)

Fig. 2. Macroscopic and microscopic observation of *T. contejeani* affected specimens: A: *Austropotamobius pallipes* complex severely affected by *Thelohania contejeani* with chalk-white opaque appearance of the abdominal musculature. B: Light microscopy of stained muscle imprint. SPVs with mature uninucleated spores (Us) and free binucleated mature spores (Bs). Hemacolor®100 \times . C: Histological appearance of *T. contejeani* affected skeletal muscle fibers of the pleon. The myofibres are replete by maturing stages of the microsporidia. Normal myofibres (*). Giemsa, 4 \times . D: Affected myofibres eliciting an inflammatory response with hyalinocytes infiltration and melanin deposition (arrows). Giemsa, 10 \times . E: Increased magnifications of melanised myofiber (arrow). H-E, 25 \times . F: *T. contejeani* affected myofibers in the heart (arrows). Giemsa, 4 \times . G: *T. contejeani* affected muscle fibers of the intestinal muscular lamina (arrows). H-E, 10 \times . H: Developmental stages of *T. contejeani* (arrow) between the perikarya of the abdominal ganglion of the ventral nerve chord. H-E, 4 \times . I: Increased magnification of the affected ventral ganglion. Sporophorous vesicles are visible (arrows). Giemsa, 40 \times .

3.5.2. Sporonts and sporoblasts inside sporophorous vesicles

Sporonts with a diameter of 4.5 μ m ($n = 5$), mostly diplokaryotic, presented a thickened plasma membrane separated from the wall of the sporophorous vesicles (Fig. 4B and C). This episporontal space was filled with fibrous cylindrical structures (170–200 nm in diameter) protruding from the sporontal membrane and a finely granular substance that in later stages appeared condensed in one or more (3) electron dense spongiform mass at the periphery of the SPV membrane (Fig. 4D). The sporont started its division by segmenting in daughter cells (Fig. 4E) and eventually in uninucleated sporoblasts (up to seven could be clearly seen in the SPV). The developing elongated sporoblasts inside the SPV lost the membrane-adhering tubular structures and showed a thickened electron dense wall (Fig. 4F). Cylindrical structure with fibrous appearance (diameter of 155–185 nm; $n = 20$) and smaller tubules (diameter of 75–85 nm; $n = 20$) were abundant inside the SPV space and clearly visible until mature spore formation (Fig. 4G and H). Sporoblast revealed a central single or multiple electron dense globule, the developing extrusion apparatus (electron dense polaroplast and anchoring disc) and a posterior vacuole.

3.5.3. Mature spores inside sporophorous vesicles

Mature spores were uninucleated, with a deeply stained cytoplasm (Fig. 4G and H), 9–12 turns of the polar filament with a diameter of 77 nm ($n = 10$), and a large posterior vacuole frequently collapsed in the study preparations (Fig. 4I and J). The spore capsule was composed of a thick electron-lucent endospore (78 nm; $n = 15$) and electron dense exospore (28 nm; $n = 15$), thinner at the apex (43 nm; $n = 5$). Some haploid spores showed an increased number of turns of the polar filament ranging from 13 up to 20 (Fig. 4I and J).

3.4.4. Diplokaryotic mature spores

A second route of sporogony with diplokaryotic mature spores was also recorded. In one sample from the Agna stream, rare diplokaryotic sporoblasts and mature spores with two nuclei were frequently observed intermingled between the maturing stages of the octosporous sporophorous vesicles and were not contained inside a SPV (Fig. 4K and L). They were ovoid in shape with a smooth surface and frequently slightly bended (bullet shaped) at the apex of the posterior vacuole, which was occupied by loosely packed granules. During fixation this vacuole usually subsided leading to collapse of the spore capsule external to it (Fig. 4M). The spore cytoplasm appeared deeply stained and finely granular with apical electron dense polaroplast; the spore extrusion apparatus comprised a mushroom-like anchoring disc and a polar filament (diameter 108 nm; $n = 10$) arranged in 5–6 coils (Fig. 4N). The spore wall was composed of a thin electron dense exospore (32 nm; $n = 8$) and a thick electron-lucent endospore (55 nm; $n = 8$), thinned at the apex (38 nm; $n = 5$). In a specimen from Fino stream (Fig. 4O), the majority of mature spore were binucleated and contained one by one in single vesicles resembling the vacuole-like compartment described by Lom et al. (2001), while octosporous sporophorous vesicles with uninucleated spores were present in low numbers. In this sample, merogony and sporogony were not easily detected nor was the sporoblast phase.

3.5. Amplification of SSU rDNA

Abdominal muscle tissues collected from macroscopically affected and suspected specimens, previously positively evaluated by cytology

and histology, were all amplified by generic primer set (18sf-350sr). *T. contejeani* species-specific primers (MIC5-1-MIC3-4) failed to amplify the majority of specimens collected from the Agna stream and all the specimens from the Vincerino stream, which were affected by *V. austropotamobii* sp. nov. These samples were readily detected by a generic primer set (V1f-1492r) and the direct sequencing of these amplified products was successful and originated sequences of *circa* 1070 bp. The amplification by the generic primer set (V1f-1492r) of *T. contejeani*-positive samples, previously confirmed with generic (18sf-350sr) and species-specific primers (MIC5-1-MIC3-4), was not as efficient and the direct sequencing of the amplified products (~1470 bp) produced uninterpretable electropherograms with overlapping peaks, suggestive of the presence of a heterogeneous SSU rRNA population. Although we observed the co-presence of the two microsporidian species in the same stream (Agna stream, Table 1), we only found one of the two parasites in each infected host determined by comparing the sequences obtained from the three primer sets. No evidence of co-infection in the same host was confirmed.

3.6. Cloning and sequencing of SSU rRNA gene

In order to assess *T. contejeani* and *V. austropotamobii* sp. nov. SSU rRNA variability, amplicons obtained by PCR with the primer set V1f-1492r were cloned and subsequently isolated and sequenced.

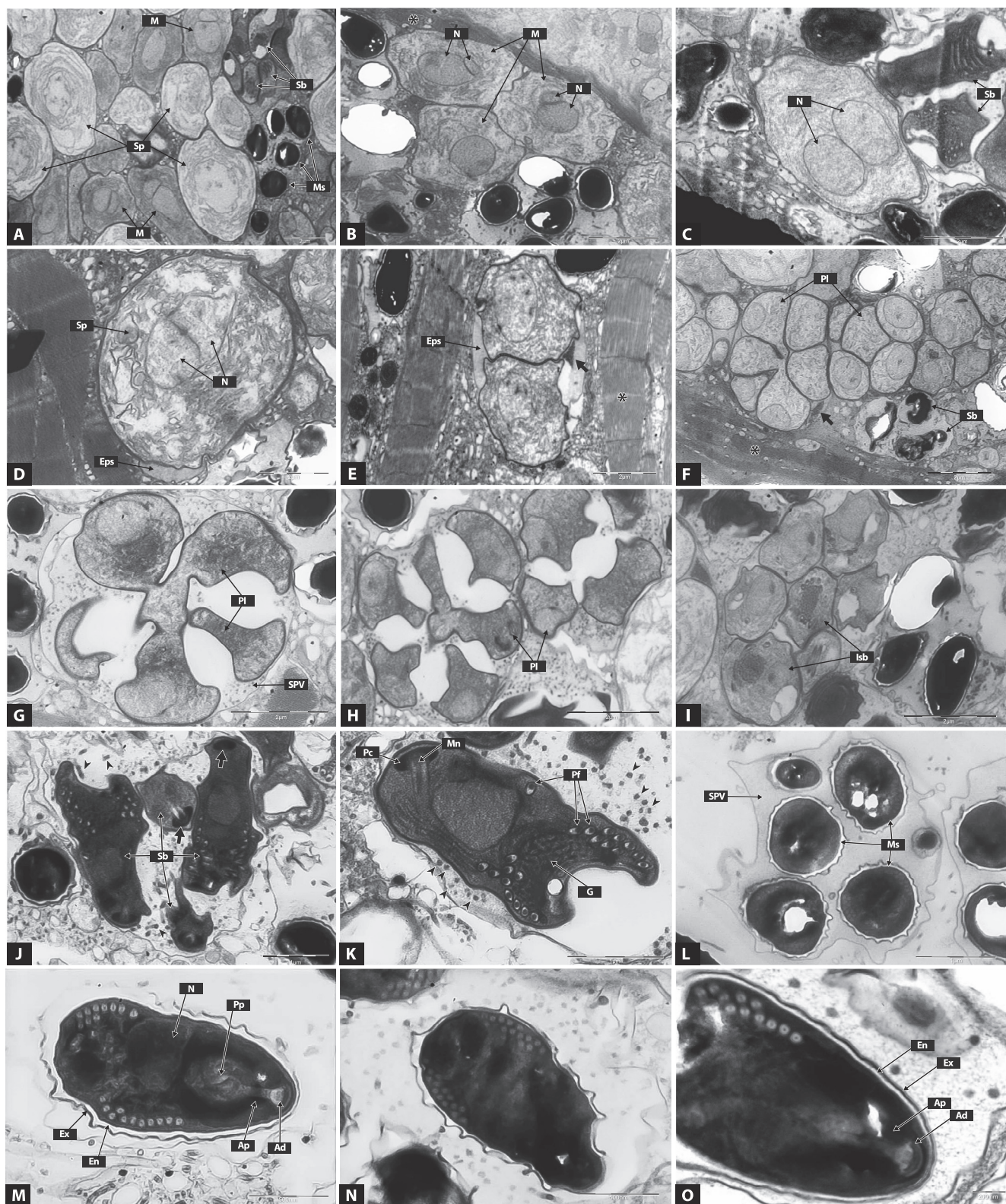
The analysis of *T. contejeani* SSU rRNA gene clones revealed the presence of two main heterogeneous variants (here named clone 1 and clone 2-like), spanning each 1318–1326 and 1267–1276 bp, for which we submitted to GenBank two representative sequences: clone 1 (Accession No. MF344630) and clone 2 (Accession No. MF344633) respectively. The observed length differences between the two variants were due to 4 deletions, observed in clone 2-like sequences, at nucleotide positions 313 (9 bp long), 342 (18 bp), 377 (21 bp) and 419 (3 bp), taking as reference *T. contejeani* clone 1 sequence. In addition, single nucleotide polymorphisms (SNPs) contributed to further variability among clone 1 and clone 2-like sequences, determining a mean identity score of 99.4% (clone 1-like sequences, $n = 5$) and 98.6% (clone 2-like sequences, $n = 9$). On the other hand, the analysis of *V. austropotamobii* sp. nov. SSU rRNA clones, for which we reported the representative sequences of clone 1 (Accession No. MF344634) and clone 2 (Accession No. MF344635), showed no length polymorphisms and a mean identity score of 99.8% ($n = 10$).

While comparing SSU rRNA sequences, *V. austropotamobii* sp. nov. showed over 99% sequence identity with the amphipod parasite *Nosema granulosis* and other insect microsporidia as *N. furnacalis*, *N. bombycis* and *V. imperfecta*, and 98% with the crayfish parasite *V. cheracis* (96% query coverage).

T. contejeani SSU rRNA clone 1-like sequences showed over 99% identity with the longer *T. contejeani* sequence of clone TcC2 (AF492593) reported by Lom et al. (2001), while clone 2-like sequences were more closely related to the shorter *T. contejeani* sequence of clone TcC3 (AF492594) (Lom et al., 2001), with 98% mean identity score.

3.7. Amplification of RPB1 gene

A fragment of the RPB1 sequence of *V. austropotamobii* sp. nov. from one specimen of Vincerino stream (Table 1) was submitted to GenBank (Accession No. MF344629). The sequence was 995 bp in length. This sequence showed 73% similarity with *N. granulosis* and 72% with *V.*



(caption on next page)

Fig. 3. Ultrastructure of *Vairimorpha austropotamobii* sp. nov. A: Different stages of development are intermingled. Meronts (M), sporonts (Sp), sporoblasts (Sb) and mature spores (Ms) inside a sporophorous vesicle. B: Putative meront stage (M), diplokaryotic cells (N) with simple plasma membrane and vacuolated cytoplasm with scarce endoplasmic reticulum. Host myofibrils (*). C: Meront with closely apposed nuclei (N) and relatively electron lucent cytoplasm. Sporoblasts (Sb). D: Diplokaryotic sporont (Sp) with condensed endoplasmic reticulum and evidence of sporophorous vesicle formation. Episporontal space (Eps). E: Uninucleated sporont daughter cells inside a sporophorous vesicle. Aggregation of electron dense granular material (arrow) is present in the episporontal space (Eps). Host striated muscle fibrils (*). F: Rosette-shaped plasmodia (Pl) showing one nucleus in each lobe. Up to six lobules visible in the section. Presence of electron dense granular material (arrow). Immature sporoblasts (Sb). G: Rosette-shaped plasmodia showing four lobes. Tubular inclusions (arrows) are evident in the cytoplasm of the SPV. H: Rosette-shaped plasmodia showing four lobes. Tubular inclusions (arrows) are evident in the cytoplasm of the SPV. I: Sporophorous vesicle with seven of eight immature uninucleated sporoblasts (Isb) visible in the section. Sporoblasts show an electron lucent posterior vacuole and electron dense granules between the first coils of the polar filament. J: Maturing elongated sporoblasts (Sb) inside a SPV with crescent shaped polar capsules (arrows) cupped around the anchoring discs. Tubular inclusions (arrowheads) are evident in the cytoplasm of the SPV. K: Detail of a maturing sporoblast showing the polar capsule (Pc), a single nucleus, the manubrium (Mn) of the polar filament (Pf), which is coiled 10 times around the collapsed posterior vacuole and sporoplasm with electron dense granules (G). L: Sporophorous vesicle containing six of eight mature spores (Ms) with a crenelated outline and electron lucent anterior vacuole. M: Mature spore with darkly stained anterior polaroplast (Ap) and lightly stained vesicular posterior polaroplast (Pp), single nucleus (N), anchoring disc (Ad) and 11 coils of the polar filament. Thick electron-lucent endospore (En) and electron-dense exospore (Ex). N: Mature spores with 13–14 coils of the polar filament. O: Detail of the apical region of a mature spore. Anchoring disc (Ad), anterior polaroplast (Ap).

←

cheracis. A fragment of the RPB1 sequence of *T. contejeani* of 912 bp from a specimen of Foce stream (Table 1) was submitted to GenBank (Accession No. MF344628).

3.8. Phylogenetic analysis

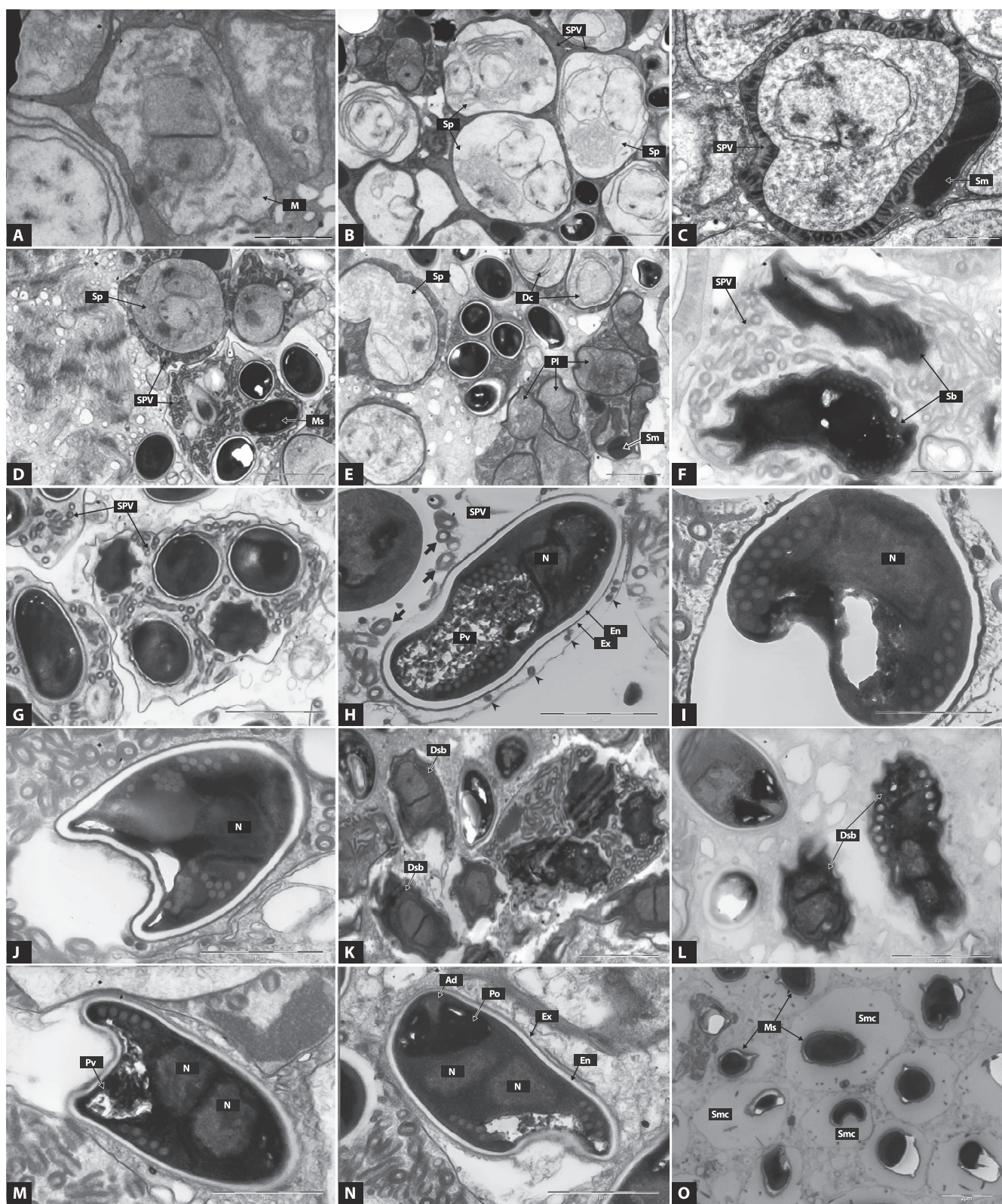
Phylogenetic analysis based on SSU rDNA sequences revealed a significant difference between *V. austropotamobii* sp. nov. and *T. contejeani* as shown in Fig. 5. The sequences of *V. austropotamobii* sp. nov. were placed in the *Nosema/Vairimorpha* group in the subclade containing *V. cheracis*, *N. granulosus* and *N. bombycis*. The sequences of *T. contejeani* were clustered together with the congeneric crayfish parasites *T. parastaci* and *T. montirivulorum*. Fig. 6 shows that phylogenetic analyses based on RPB1 sequences placed *V. austropotamobii* sp. nov. among species of the clade *Nosema/Vairimorpha* and *T. contejeani* close related with members of the Class Terresporidia. *V. austropotamobii* sp. nov. did not cluster together either with *N. bombycis* or with *V. necatrix*.

4. Discussion

4.1. Ultrastructural characterization of *V. austropotamobii* sp. nov.

In this study we confirmed the presence of *T. contejeani* in crayfish that were macroscopically representative of porcelain disease but we also identified a new octosporoblastic microsporidian parasite, *Vairimorpha austropotamobii* sp. nov., which shows a similar muscular tropism in *A. pallipes* complex. In the work by Moodie et al. (2003c) the features of the species *V. cheracis* had been carefully compared to the type species *V. necatrix* and the reasons for placing this species in the genus *Vairimorpha* had been discussed. A significant part of those considerations may apply to the new species herein described. Therefore, *Vairimorpha austropotamobii* sp. nov. has been placed in the genus *Vairimorpha* due to ultrastructural and genetic similarities with the species *V. cheracis* (Moodie et al., 2003c) and *V. necatrix*. The species name “*austropotamobii*” refers to the crustacean host in which the parasite was found, *Austropotamobius pallipes* complex. The ultrastructural and developmental features of the octosporoblastic sequence, shared between the type species *V. necatrix* and both *V. cheracis* and *V. austropotamobii* sp. nov. include the diplokaryotic nature of the sporonts, the formation of a SPV around the dividing sporont prior to cytokinesis of the sporont daughter cells and the presence of electron dense material in the episporontal space, which appears to be associated with deposition of an electron dense layer on the outside of the rosette-shaped sporogonial plasmodium. As described in *V. cheracis*, the electron dense inclusions of *V. austropotamobii* sp. nov. were not as numerous as the ones in the SPVs of *V. necatrix* (Mitchell and Cali, 1993) or *V. imperfecta* (Canning et al., 1999) and did not form concentric layers. The separation of the nuclei prior to division of the sporont into two uninucleate cells, as described in the type species, was observed also in *V. austropotamobii* sp. nov. The plasmodium observed in *V. austropotamobii* sp. nov., showed up to four contiguous lobes. This finding is consistent with the development of two tetralobated

plasmodia inside the SPV as proposed for the type species. Maturing sporoblast of *V. austropotamobii* sp. nov. and *V. cheracis* showed at the posterior pole of the maturing sporoblast an electron dense granular sporoplasm between the posterior vacuole and the coils of the polar filament. Ultrastructural features of the uninucleate spores shared by *V. austropotamobii* sp. nov., *V. cheracis* and *V. necatrix* included the isofilar nature of the polar tube, a bipartite polaroplast with darkly-stained anterior and lightly-stained vesicular posterior appearance, and the morphology of the anchoring disc. Similar numbers of coils of the polar filament occurred in mature octospores; 11–14 in *V. austropotamobii* sp. nov., 10–12 in *V. cheracis* and 13–14 in *V. necatrix*. The type description for *V. necatrix* included dimorphic development, with both disporoblastic diplokaryotic sporogony and octosporoblastic haploid sporogony occurring in the lepidopteran host (Pilley, 1976). Only the latter form of monokaryotic sporogony was observed in white-clawed crayfish heavily infected with *V. austropotamobii* sp. nov. In the genera *Vairimorpha* and *Nosema*, including the type species *V. necatrix* and *N. bombycis*, the purpose of primary binucleate spores is parasite dissemination to different tissues (Solter and Maddox, 1998). Considering the advanced stage of infection in the ultrastructurally analyzed crayfish, it cannot be excluded that *V. austropotamobii* sp. nov. has an early disporoblastic sequence resulting in binucleate spores. Previous studies (Pilley, 1976; Mitchell and Cali, 1993) found that octosporoblastic sporogony of *V. necatrix* with production of haploid meiospores was more frequent at low ambient temperatures, most notably below 20 °C, coupled with a decrease in frequency of diplokaryotic spores. A similar finding was reported for *V. mesnilii* (Malone and McIvor, 1996) and for *V. plodiae* (Malone and Canning, 1982). The habitat of the crayfish host *A. pallipes* complex, collected in small mountain streams (450–500 m a.s.l.), provides a relatively cool water temperature (12–18 °C) also in the summer. As suggested by Moodie et al. (2003c) for *V. cheracis* identified in *C. destructor* collected from the highland of New South Wales, low water temperature and the advanced stage of infection observed in the crayfish host might explain the only evidence of the monokaryotic sporogony of these crustacean-affecting *Vairimorpha* species. Evaluations on the effects of higher water temperatures on sporogony of *V. austropotamobii* sp. nov. in recently infected white-clawed crayfish might reveal the presence of a sporogony sequence resulting in diplokaryotic spores putatively connected to within-host transmission of the parasite. Histological analyses of affected crayfish revealed that mature spores inside a SPV and earlier developmental stages of *V. austropotamobii* sp. nov. were exclusively found in striated muscle tissue. The lack of histological evidence of maturing stages in the musculature of the gut, in the ovarian tissue or the presence of spores in the haemocytes, or free in the haemolymph, could indicate that uninucleated spores in the SPV are formed by horizontal transmission mainly through cannibalism or ingestion of spores released by lysis of the musculature at the death of the host. The relatively persistent SPV, as observed in fresh muscle imprints preparations, might help to maintain the viability and infectivity of spores after death of the parasitised crayfish and during the transit through the digestive system of the next host. It is possible that an intermediate host is involved in



(caption on next page)

Fig. 4. Ultrastructure of *Thelohania contejeani* A: Meront with adhering diplokarya and simple plasmalemma (M). B: Binucleated sporonts (Sp) with thickened plasmalemma, evident endoplasmic reticulum, each contained in the developing sporophorous vesicle (SPV). Initial fibrous tubules are visible, attached on the sporont plasmalemma. C: Mature sporont inside a SPV with prominent fibrous tubules projecting from the sporont plasmalemma and single electron-dense spongiform mass (Sm). D: Sporophorous vesicles at different development stages. SPV with mature binucleate sporont (Sp) with spongiform mass, SPV with initial segmentation of the sporont (arrow), and SPV with mature spores (Ms). Episporontal space filled with fibrous tubules. E: Segmenting sporonts inside the SPVs characterized by initial division in two daughter cell (Dc) inside the SPV and subsequent segmentation of the sporogonial plasmodia (Pl) into uninucleate sporoblasts. One SPV presents three dense spongiform masses (Sm). F: Maturing elongated sporoblasts (Sb) inside the SPV. Abundance of fibrous tubules. G: Sporophorous vesicle with five of eight mature spores. H: Mature uninucleate spore inside a SPV with 13 turns of the polar filament and a posterior vacuole (Pv) with loosely packed granules, thick electron-lucent endospore (En) and dense exospore (Ex). Fibrous macrotubules (arrow) and smaller tubules (arrowheads) are evident in the SPV. I: Mature uninucleate spore, inside a SPV, with 15 turns of the polar filament and a collapsed posterior vacuole. The polar filament in transverse section reveals an electron dense ring and an electron dense core. J: Mature uninucleate spore, inside a SPV, with 20 turns of the polar filament and a collapsed posterior vacuole. K: Single diplokaryotic sporoblasts (Dsb) are arranged around a SPV with monokaryotic sporoblasts. L: Maturing diplokaryotic sporoblasts (Dsb) with 5 turns of the polar filament. M: Mature binucleate spore with 5 turns of the polar filament intermingled between SPVs. Collapsed posterior vacuole (Pv), darkly stained anterior polaroplast, nuclei (N). N: Mature binucleate spore with 6 turns of the polar filament. Collapsed posterior vacuole, darkly stained anterior polaroplast (Po), anchoring disc (Ad) and finely granular sporoplasma. O: Binucleate mature spores (Ms) contained inside single membrane compartments (Smc).

horizontal transmission of *V. austropotamobii* sp. nov. The fate of monokaryotic spores produced by species of the genus *Vairimorpha* has not been documented in natural environment, and it is not known whether transmission is strictly direct or involves an intermediate host (Ironside, 2007). Studies on the genera *Amblyospora*, *Hyalinocysta* and *Duboscquia*, parasitic in mosquito hosts, revealed that a copepod intermediate host was involved in transmission of uninucleate spores to the next mosquito host (Sweeney et al., 1993; Andreadis, 2005). The inclusion of an intermediate host in the life cycle might help to ensure survival of microsporidia in temporary aquatic environments subject to abrupt changes, i.e. drought (Andreadis and Vossbrinck, 2002).

4.2. Phylogenetic analysis of *V. austropotamobii* sp. nov.

The results of both SSU rRNA and RPB1 genes are consistent in placing *V. austropotamobii* sp. nov. in the Class Terresporidia following the classification proposed by Vossbrinck and Debrunner-Vossbrinck (2005), between members of the genera *Nosema*/*Vairimorpha*, closely related to *N. granulosus*, *N. furnacalis* and *V. cheracis*. Although *V. austropotamobii* sp. nov. shows over 99% sequence similarity with *N. granulosus* of the conserved SSU rRNA gene, it clearly differentiates from *N. granulosus* for the RPB1 sequence (73% similarity) and also for the life cycle, host, tissue tropism and sporogony sequence. *Nosema granulosus* infects amphipods of the genus *Gammarus*, has no evidence of horizontal transmission, does not cause patent pathology, being restricted to the ovarian tissues, and relies on efficient transovarial transmission and feminization of the host progeny (Terry et al., 1998). Considering the SSU rRNA gene, *V. austropotamobii* sp. nov. appears phylogenetically more distantly related to the *Vairimorpha* type species *V. necatrix*, and to other members of its subclade, than to members of the subclade that included the *Nosema* type species *Nosema bombycis*. However, the phylogeny of the single-copy RPB1 gene does not cluster *V. austropotamobii* sp. nov. with any type species of the two subclades. Therefore, as phylogenetic placement does not assign it unequivocally to the *N. bombycis* subclade, we considered significant that from a morphological prospective the presence of an octosporoblastic sporogony sequence precluded placement of *V. austropotamobii* sp. nov. in the genus *Nosema*, according to its type description that includes only diplosporoblastic sporogony resulting in binucleate spores without presence of sporophorous vesicle (Sprague et al., 1992), and substantiates the inclusion in the genus *Vairimorpha*.

4.3. Considerations regarding *T. contejeani*

The life cycle of the three *Thelohania* spp. described in crayfish hosts is similar to that of the genus *Vairimorpha*, presenting both diplokaryotic and monokaryotic phases, but differs from congeneric *Thelohania* species affecting other marine crustacean hosts that appear monomorphic (*T. maenadis* Perez, 1904; *T. octospora* Henneguy, 1892 (Vivares, 1980); *T. butleri* (Brown and Adamson, 2006)). In the review of the taxonomic affinities of *T. contejeani* conducted by Lom et al. (2001), and to a broader extent by Moodie et al. (2003b), it has been stated that simultaneous dimorphic sporogony and a sporogonic development

characterized by rosette-like plasmodia are features not related to the genus *Thelohania* following the classification proposed by Gurley (1893) and Hazard and Oldacre (1975). A series of three binary fissions of the sporont (without the formation of a plasmodium inside the SPV), which had originally been described by microscopic observation in the *Thelohania* type species *Thelohania giardi*, parasite of *Crangon crangon* (Henneguy and Theohan, 1892) and only recently confirmed by ultrastructural examination in *T. butleri*, parasite of the marine shrimp *Pandalus jordani* (Brown and Adamson, 2006), should be considered the typical development in the genus *Thelohania*. SSU rRNA phylogeny previously conducted by other authors (Vossbrinck and Debrunner-Vossbrinck, 2005; Stentiford et al., 2013) could not unambiguously resolve the position of the crayfish *Thelohania* spp. within one of the major three Classes Aquasporidia, Terresporidia and Marinospordia. In the work by Moodie et al. (2003b) crayfish *Thelohania* spp. were grouped together, thus suggesting a host-parasite co-speciation, and appeared as a sister clade to the *Nosema*/*Vairimorpha* group, between members of the subsequently defined Class Terresporidia (Vossbrinck and Debrunner-Vossbrinck, 2005). In our phylogeny conducted by Maximum likelihood the three *Thelohania* spp. from crayfish cluster together and are moderately related with other Terresporidia, whereas they appear clearly separated from the marine congeneric *T. butleri*, placed with other marine crustacean and fish microsporidia in the Class Marinospordia. The RPB1 phylogeny, although based on a reduced number of species, confirms the distance of *T. contejeani* from the Class Marinospordia and Aquasporidia and the relatedness with microsporidia ascribed in the Class Terresporidia. These morphological and phylogenetic considerations highlight the need for a taxonomic revision of the genus *Thelohania* and family Thelohaniidae, primarily based on molecular and fine ultrastructural data of the type species *T. giardi*. This will likely result in a taxonomic separation of the freshwater crayfish microsporidia from the marine species. The evidence of two variants of SSU rRNA gene in *T. contejeani*, that differs for two deletions, has been previously described by Lom et al. (2001). In our study we confirmed the presence of at least two variants of the gene that markedly differ in length due to multiple deletions, but we also observed the presence of significant nucleotide diversity between copies of the gene that shows these deletions. This finding had already been described in other microsporidian species and thoroughly investigated in the *Nosema*/*Vairimorpha* group by Ironside (2013), who demonstrated intergenomic and intragenomic diversity of rDNA sequences within isolates of microsporidia acquired from single hosts. In our material ultrastructural observation of *T. contejeani* uninucleated mature spores showed a high variation in the number of coils of the polar filament, from 9 to 20 turns, in comparison with the description by Lom et al. (2001), which was restricted to 9–11 turns. This variability was also observed in uninucleated spores of *T. parastaci* (12–20 turns) (Moodie et al., 2003a).

4.4. Differentiating *V. austropotamobii* sp. nov. from *T. contejeani*

The diagnostic criteria to differentiate *V. austropotamobii* sp. nov from *T. contejeani* are tissue tropism, the ratio of free spores and SPVs in muscle imprints and ultrastructural appearance of SPV and mature

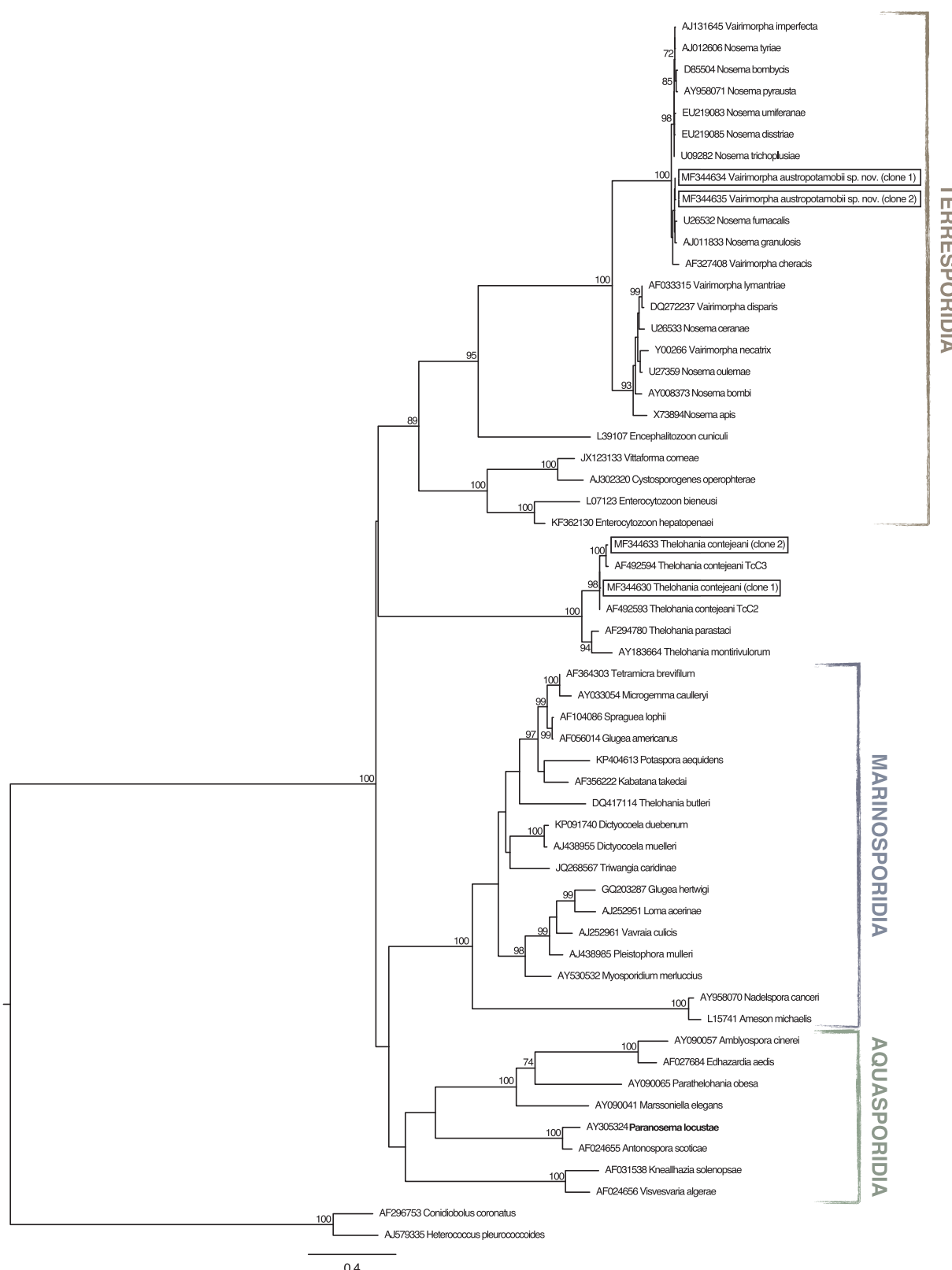


Fig. 5. Maximum likelihood phylogenetic tree based on SSU rRNA gene sequences. The phylogenetic tree shows the relationship of *Vairimorpha austropotamobii* sp. nov. and *Thelohania contejeani* with other microsporidia of the Classes Terresporidia, Marinosporidia and Aquasporidia. The numbers at the nodes represent bootstrap values (only values $\geq 70\%$ are reported), while branch lengths are scaled according to the number of nucleotide substitutions per site. The scale bar is reported.

spores. *V. austropotamobii* sp. nov. does not affect the heart, the intestinal musculature nor the ganglia of the ventral nerve chord and does not elicit inflammation and melanisation. The proportion between sporoblasts and mature spores contained inside a SPV and free spores is

notably higher in *V. austropotamobii* sp. nov. than in *T. contejeani*. Conversely, the presence of macrotubules of large diameter (155–185 nm) with fibrous and coiled appearance in the episporontal space of the SPV and protruding from the sporontal membrane is

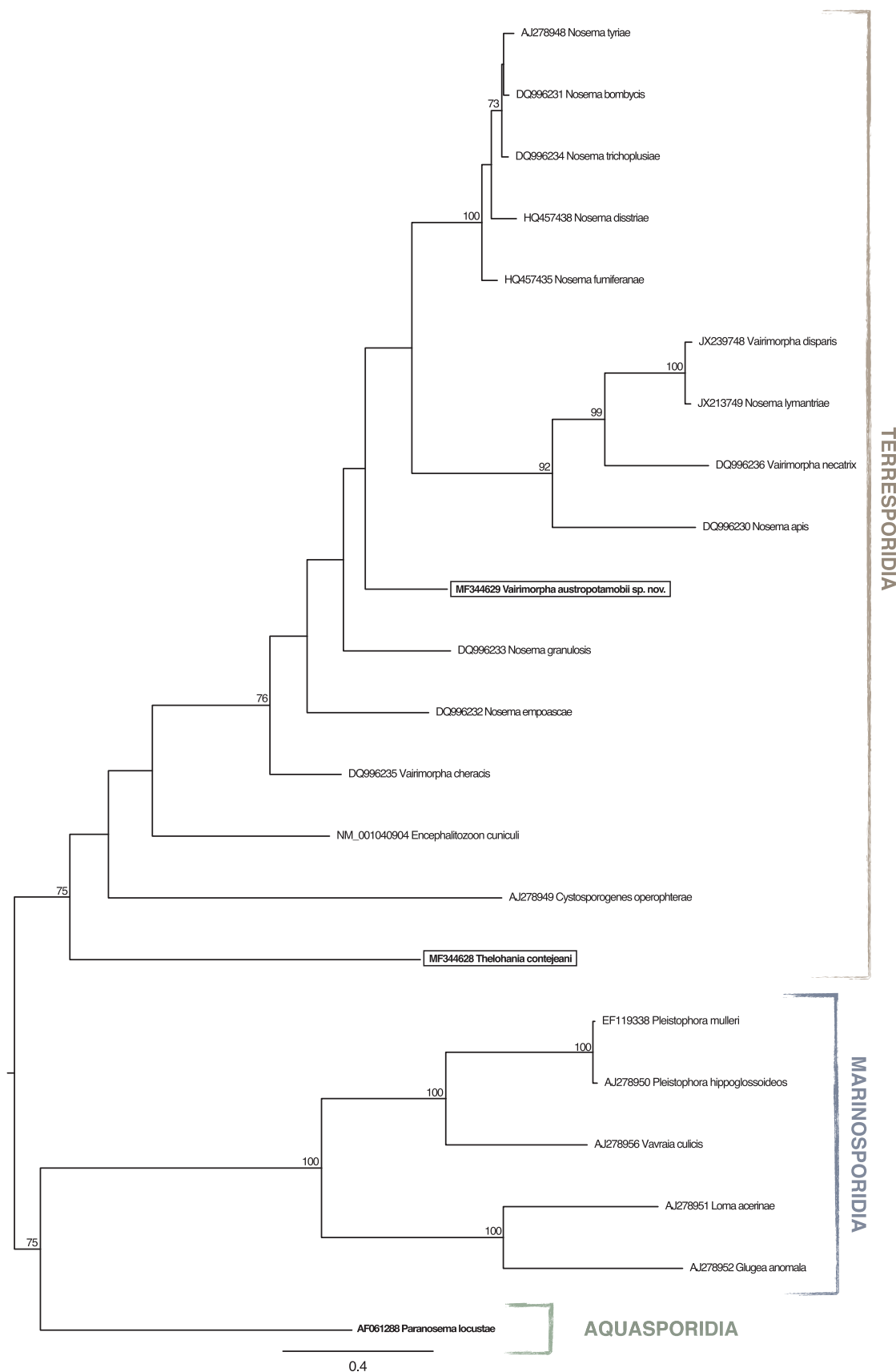


Fig. 6. Maximum likelihood phylogenetic tree based on RPB1 gene sequences. The phylogenetic tree shows the relationship of *Vairimorpha austropotamobii* sp. nov. and *Thelohania contejeani* with other microsporidia of the Classes Terresporidia, Marinospordia and Aquasporidia. The numbers at the nodes represent bootstrap values (only values $\geq 70\%$ are reported), while branch lengths are scaled according to the number of nucleotide substitutions per site. The scale bar is reported.

evident only in *T. contejeani*. *V. austropotamobii* sp. nov. appears monomorphic whereas *T. contejeani* is dimorphic with octosporous vesicles with uninucleate spores and diplokaryotic free spores. Molecular identification is best performed via amplification by generic primer set (18sf-350sr) (Baker et al., 1995) and sequencing of the amplified product. Although *V. austropotamobii* sp. nov. does not affect the heart, it can cause severe impairment to the musculature and clearly reduce the overall fitness of the affected crayfish. Further studies are needed to evaluate the progression of the pathology and the life span of early-infected specimens. The presence of affected crayfish during three years of monitoring in the same location (Vincerino stream; years 2012–2015) indicates a consistent circulation and maintenance of the microsporidia in the host population. Alternative hosts and transmission routes in the life cycle of *V. austropotamobii* should be investigated in order to reduce the possible spread of this new pathogen from affected to naïve populations of the endangered white-clawed crayfish.

Taxonomic summary – *Vairimorpha austropotamobii* sp. nov. (Pretto).

Type host: the freshwater crayfish *Austropotamobius pallipes* complex (Lereboullet, 1858), subspecies *Austropotamobius italicus carsicus*.

Transmission: unknown.

Site of infection: skeletal muscle tissue of male and female host.

Host-parasite interface: meronts and early sporonts in direct contact with host cell cytoplasm. Uninucleate spores produced inside a sporophorous vesicle of parasite origin.

Merogony: diplokaryotic meronts, round in shape (diameter 4.6 µm).

Transition to sporogony: ovoid diplokaryotic sporont (5.9 × 4.1 µm) with a thickened plasmalemma and increased endoplasmic reticulum.

Sporogony: only octosporoblastic sporogony observed. Sporont divides into two uninucleate cells within the sporophorous vesicle. Each daughter cell forms a rosette-shaped plasmodium and divides in four sporoblasts. Eight uninucleated sporoblast mature within a sporophorous vesicle.

Sporophorous vesicles: of parasite origin, spherical in shape, with an average diameter of 7.9 (7.5–8.3 µm) (n = 50). Tubular-like structures within SPV are 84 nm (n = 10) in diameter.

Spore: only uninucleated pyriform spores observed. Average fresh spore length: 3.9 (3.5–4.3 µm). Average fresh spore width 2.2 (1.9–2.5 µm) (n = 50). Lateral exospore width: 34 nm (n = 10), lateral endospore width: 54 nm, apical endospore width: 27 nm (n = 4). Layered exospore wall. Isofilar polar filament with 11–14 coils and diameter of 74 nm (n = 20). Anterior electron-dense polaroplast, posterior vesicular polaroplast. Posterior vacuole of moderate dimension. The spore capsule appears crenelated in ultrastructural observation.

Type locality: Vincerino stream (45°42'–10°37'), Lombardy region, Italy.

Type specimens: histological sections and ethanol-fixed affected tissues were deposited in the Veterinary Biobank of the Istituto Zooprofilattico Sperimentale delle Venezie (IZSVe). Submission code: IZSVe FUN CC LL 1.

Molecular data: SSU rDNA cloned and sequenced, GenBank accession number: MF344634, MF344635. Part of the large sub-unit RNA polymerase II (RPB1) sequenced directly and included in GenBank accession: MF344629.

Remarks: only heavily infected adult white-clawed crayfish were sampled.

Acknowledgments

This study was partially supported by the European Funds through Financial Instrument for the Environment, LIFE+ (LIFE 08 NAT/IT/000352 – CRAINat) and (LIFE+ 10 NAT/IT/000239 – RARITY). The authors would like to thank Dr. Anna Toffan for manuscript revision, Ms Francesca Ellero for proof reading, Mr Andrea Vernucci for tables

layout and two anonymous referees for comments on the original manuscript.

Conflict of interest

None.

References

- Andreadis, T.G., 2005. Evolutionary strategies and adaptations for survival between mosquito-parasitic microsporidia and their intermediate copepod hosts: a comparative examination of *Amblyospora connectus* and *Hyalinocysta chapmani* (Microsporidia: Amblyosporidae). *Folia Parasitol. (Praha)* 52 (1–2), 23–35.
- Andreadis, T.G., Vossbrinck, C.F., 2002. Life cycle, infrastructure and molecular phylogeny of *Hyalinocysta chapmani* (Microsporidia: Thelohaniidae), a parasite of *Culiseta melanura* (Diptera: Culicidae) and *Orthocyclops modestus* (Copepoda: Cyclopidae). *J. Eukaryot. Microbiol.* 49, 350–364. <http://dx.doi.org/10.1111/j.1550-7408.2002.tb00382.x>.
- Baker, M.D., Vossbrinck, C.R., Didier, E.S., Maddox, J.V., Shadduck, J.A., 1995. Small-subunit ribosomal DNA phylogeny of various microsporidia with emphasis on AIDS-related forms. *J. Eukaryot. Microbiol.* 42, 564–570.
- Bernini, G., Bellati, A., Pellegrino, I., Negri, A., Ghia, D., Fea, G., Sacchi, R., Nardi, P.A., Fasola, M., Galeotti, P., 2016. Complexity of biogeographic pattern in the endangered crayfish *Austropotamobius italicus* in northern Italy: molecular insights of conservation concern. *Conserv. Genet.* 17, 141–154.
- Brown, A.M.V., Adamson, M.L., 2006. Phylogenetic distance of *Thelohania butleri* Johnston, Vernick, and Sprague, 1978 (Microsporidia: Thelohaniidae), a parasite of the smooth pink shrimp *Pandalus jordani*, from its congener suggests need for major revision of the genus *Thelohania* Henneguy, 1892. *J. Eukaryot. Microbiol.* 53, 445–455. <http://dx.doi.org/10.1111/j.1550-7408.2006.00128.x>.
- Canning, E.U., Curry, A., Cheney, S., Lafranchi-Tristem, N.J., Haque, M.A., 1999. *Vairimorpha imperfecta* n. sp., a microsporidian exhibiting an abortive octosporous sporogony in *Plitella xylostea* L. (Lepidoptera: Yponomeutidae). *Parasitology* 119 (3), 273–286.
- Cheney, S.A., Lafranchi-Tristem, N.J., Bourges, D., Canning, E.U., 2001. Relationships of microsporidian genera, with emphasis on the polysporous genera, revealed by sequences of the largest subunit of RNA polymerase II (RPB1). *J. Eukaryot. Microbiol.* 48 (1), 111–117.
- Cossins, A.R., Bowler, K., 1974. An histological and ultrastructural study of *Thelohania contejeani* Henneguy, 1892 (Nosematidae), Microsporidian parasite of the crayfish *Austropotamobius pallipes* Lereboullet. *Parasitology* 68, 81–91. <http://dx.doi.org/10.1017/S003118200004539X>.
- Darriba, D., Taboada, G.L., Doallo, R., Posada, D., 2012. jModelTest 2: more models, new heuristics and high-performance computing. *Nat. Methods* 9<http://dx.doi.org/10.1038/nmeth.2109>. 772–772.
- Dunn, J.C., McClymont, E.H., Christmas, M., Dunn, A.M., 2009. Competition and parasitism in the native White Clawed Crayfish *Austropotamobius pallipes* and the invasive Signal Crayfish *Pacifastacus leniusculus* in the UK. *Biol. Invasions* 11, 315–324. <http://dx.doi.org/10.1007/s10530-008-9249-7>.
- Edgerton, B.F., Evans, L.H., Stephens, F.J., Overstreet, R.M., 2002. Synopsis of freshwater crayfish diseases and commensal organisms. *Aquac. Ann. Rev. Fish Dis.* 9 (206), 57–135. [http://dx.doi.org/10.1016/S0044-8486\(01\)00865-1](http://dx.doi.org/10.1016/S0044-8486(01)00865-1).
- Endrizzi, S., Bruno, M.C., Maiolini, B., 2013. Distribution and morphometry of native and alien crayfish in Trentino (Italy). *J. Limnol.* 72, 343–360. <http://dx.doi.org/10.4081/jlimnl.2013.e28>.
- France, R.L., Graham, L., 1985. Increased microsporidian parasitism of the crayfish *Orconectes virilis* in an experimentally acidified lake. *Water Air Soil Pollut.* 26, 129–136. <http://dx.doi.org/10.1007/BF00292063>.
- Fratini, S., Zaccara, S., Barbaresi, S., Grandjean, F., Souty-Grosset, C., Crosa, G., Gherardi, F., 2005. Phyleogeography of the threatened crayfish (genus *Austropotamobius*) in Italy: implications for its taxonomy and conservation. *Heredity* 94, 108–118.
- Guindon, S., Dufayard, J.F., Lefort, V., Anisimova, M., Hordijk, W., Gascuel, O., 2010. New algorithms and methods to estimate maximum-likelihood phylogenies: assessing the performance of PhyML 3.0. *Syst. Biol.* 59, 307–321. <http://dx.doi.org/10.1093/sysbio/syq010>.
- Gurley, R., 1893. On the classification of the Myxosporidia, a group of protozoan parasites infesting fishes. *Bull. US Dep. Agric.* 11, 407–420.
- Hazard, E.I., Oldacre, S.W., 1975. Revision of microsporida (Protozoa) close to *Thelohania*, with descriptions of one new family, eight new genera, and thirteen new species. *Bull. US Dep. Agric.* 1530, 1–104.
- Henneguy, G., Thelohan, P., 1892. Myxosporides parasites des muscles chez quelques crustaces decapodes. *Ann. Microgr.* 4, 617–641.
- Herbert, B.W., 1988. Infection of *Cherax quadricarinatus* (Decapoda: Parastacidae) by the microsporidium *Thelohania* sp. (Microsporidia: Nosematidae). *J. Fish Dis.* 11, 301–308. <http://dx.doi.org/10.1111/j.1365-2761.1988.tb01226.x>.
- Hillis, D.M., Dixon, M.T., 1991. Ribosomal DNA: molecular evolution and phylogenetic inference. *Q. Rev. Biol.* 66, 441–453.
- Imhoff, E.M., Mortimer, R.J.G., Christmas, M., Dunn, A.M., 2010. Non-lethal tissue sampling allows molecular screening for microsporidian parasites in signal *Pacifastacus leniusculus* (Dana) and white-clawed crayfish, *Austropotamobius pallipes* (Lereboullet). *Freshw. Crayfish* 17, 145–150.
- Ironside, J.E., 2013. Diversity and recombination of dispersed ribosomal DNA and protein coding genes in Microsporidia. *PLoS ONE* 8 (2), e55878. <http://dx.doi.org/10.1371>

- journal.pone.0055878.
- Ironside, J.E., 2007. Multiple losses of sex within a single genus of Microsporidia. *BMC Evol. Biol.* 7, 48. <http://dx.doi.org/10.1186/1471-2148-7-48>.
- Jelić, M., Klobučar, G.I.V., Grandjean, F., Puillandre, N., Franjević, D., Futo, M., Amouret, J., Maguire, I., 2016. Insights into the molecular phylogeny and historical biogeography of the white-clawed crayfish (Decapoda, Astacidae). *Mol. Phylogenetic Evol.* 103, 26–40. <http://dx.doi.org/10.1016/j.ympev.2016.07.009>.
- Jones, J.B., 1980. Freshwater crayfish *Paraneoprops planifrons* infected with the microsporidian *Thelohania*. *N. Z. J. Mar. Freshw. Res.* 14, 45–46.
- Loon, J., Nilsen, F., Dykova, I., 2001. *Thelohania contejeani* Henneguy, 1892: dimorphic life cycle and taxonomic affinities, as indicated by ultrastructural and molecular study. *Parasitol. Res.* 87, 860–872.
- Longshaw, M., 2011. Diseases of crayfish: a review. *Dis. Edible Crustac.* 106, 54–70. <http://dx.doi.org/10.1016/j.jip.2010.09.013>.
- Malone, L.A., Canning, E.U., 1982. Fine structure of *Vairimorpha plodiae* (Microspora, Burenellidae), a pathogen of *Plodia interpunctella* (Lepidoptera, Phycitidae) and infectivity of the dimorphic spores. *Protistologica* 18, 503–516.
- Malone, L.A., McIvor, C.A., 1996. Use of nucleotide sequence data to identify a Microsporidian pathogen of *Pieris rapae* (Lepidoptera, Pieridae). *J. Invertebr. Pathol.* 68, 231–238. <http://dx.doi.org/10.1006/jipa.1996.0090>.
- McGriff, D., Modlin, J., 1983. *Thelohania contejeani* parasitism of the crayfish, *Pacifastacus leniusculus*, in California. *Calif. Fish Game* 69, 178–183.
- McManus, D.P., Bowles, J., 1996. Molecular genetic approaches to parasite identification: their value in diagnostic parasitology and systematics. *Int. J. Parasitol.* 26, 687–704. [http://dx.doi.org/10.1016/0020-7519\(96\)82612-9](http://dx.doi.org/10.1016/0020-7519(96)82612-9).
- Mitchell, M.J., Cali, A., 1993. Ultrastructural study of the development of *Vairimorpha necatrix* (Kramer, 1965) (Protozoa, Microsporida) in larvae of the corn earworm, *Heliothis zea* (Boddie) (Lepidoptera, Noctuidae) with emphasis on sporogony. *J. Eukaryot. Microbiol.* 40, 701–710. <http://dx.doi.org/10.1111/j.1550-7408.1993.tb0462.x>.
- Moodie, E.G., Le Jambre, L.F., Katz, M.E., 2003a. *Thelohania parastaci* sp. nov. (Microspora: Thelohaniidae), a parasite of the Australian freshwater crayfish, *Cherax destructor* (Decapoda: Parastacidae). *Parasitol. Res.* 91, 151–165.
- Moodie, E.G., Le Jambre, L.F., Katz, M.E., 2003b. *Thelohania montivulorum* sp. nov. (Microspora: Thelohaniidae), a parasite of the Australian freshwater crayfish, *Cherax destructor* (Decapoda: Parastacidae): fine ultrastructure, molecular characteristics and phylogenetic relationships. *Parasitol. Res.* 91, 215–228. <http://dx.doi.org/10.1007/s00436-003-0948-9>.
- Moodie, E.G., Le Jambre, L.F., Katz, M.E., 2003c. Ultrastructural characteristics and small subunit ribosomal DNA sequence of *Vairimorpha cheracis* sp. nov. (Microspora: Burenellidae), a parasite of the Australian yabby, *Cherax destructor* (Decapoda: Parastacidae). *J. Invertebr. Pathol.* 84, 198–213. <http://dx.doi.org/10.1016/j.jip.2003.11.004>.
- Mori, M., Salvidio, S., 2000. The occurrence of *Thelohania contejeani* Henneguy, a microsporidian parasite of the crayfish *Austropotamobius pallipes* (Lereboullet), in Liguria Region (NW Italy). *J. Limnol.* 59, 165–167.
- Oidtmann, B., El-Matbouli, M., Fischer, H., Hoffmann, R., Klarding, K., Schmid, I., Schmidt, R., 1996. Light microscopy of *Astacus astacus* L. under normal and selected pathological conditions, with special emphasis to porcelain disease and crayfish plague. *Freshw. Crayfish* 11, 465–480.
- Pilley, B.M., 1976. New genus, *Vairimorpha* (Protozoa-Microsporida), for *Nosema necatrix* Kramer 1965 – pathogenicity and life-cycle in *Spodoptera exempta* (Lepidoptera-
- Noctuidae). *J. Invertebr. Pathol.* 28, 177–183.
- Quaglio, F., Capovilla, P., Fioravanti, M.L., Marino, F., Gaglio, G., Florio, D., Fioretto, B., Gustinelli, A., 2011. Histological analysis of thelohaniasis in white-clawed crayfish *Austropotamobius pallipes* complex. *Knowl. Manag. Aquat. Ecosyst.* 401, 11. <http://dx.doi.org/10.1051/kmae/2011045>.
- Quilter, C.G., 1976. Microsporidian parasite *Thelohania contejeani* Henneguy from New Zealand freshwater crayfish. *N. Z. J. Mar. Freshw. Res.* 10, 225–231.
- Sogandares-Bernal, F., 1962. Presumable microsporidiosis in the dwarf crayfishes *Cambarellus puer* Hobbs and *C. shufeldti* (Faxon) in Louisiana. *J. Parasitol.* 48 <http://dx.doi.org/10.2307/3275225>, 493–493.
- Solter, L.F., Maddox, J.V., 1998. Physiological host specificity of Microsporidia as an indicator of ecological host specificity. *J. Invertebr. Pathol.* 71, 207–216. <http://dx.doi.org/10.1006/jipa.1997.4740>.
- Sprague, V., 1950. *Thelohania cambarii* n. sp., a microsporidian parasite of North American crayfish. *J. Parasitol.* 36, 46.
- Sprague, V., Becnel, J.J., Hazard, E.I., 1992. Taxonomy of phylum microspora. *Crit. Rev. Microbiol.* 18, 285–395 (5–6).
- Stentiford, G.D., Feist, S.W., Stone, D.M., Bateman, K.S., Dunn, A.M., 2013. Microsporidia: diverse, dynamic, and emergent pathogens in aquatic systems. *Trends Parasitol.* 29, 567–578. <http://dx.doi.org/10.1016/j.pt.2013.08.005>.
- Sweeney, A.W., Doggett, S.L., Piper, R.G., 1993. Life cycle of a new species of Duboscquia (Microsporida: Thelohaniidae) infecting the mosquito *Anopheles hilli* and an intermediate copepod host, *Apocyclops dengizicus*. *J. Invertebr. Pathol.* 62, 137–146. <http://dx.doi.org/10.1006/jipa.1993.1089>.
- Tamura, K., Peterson, D., Stecher, G., Nei, M., Kumar, S., 2011. MEGA5: molecular evolutionary genetics analysis using maximum likelihood, evolutionary distance, and maximum parsimony methods. *Mol. Biol. Evol.* 28, 2731–2739. <http://dx.doi.org/10.1093/molbev/msr121>.
- Tangprasittipap, A., Srivasa, J., Chouwdee, S., Somboon, M., Chuchird, N., Limsuwan, C., Srivatan, T., Flegel, T.W., Sritunyalucksana, K., 2013. The microsporidian *Enterocytozoon hepaticenae* is not the cause of white feces syndrome in whiteleg shrimp *Penaeus (Litopenaeus) vannamei*. *BMC Vet. Res.* 9 <http://dx.doi.org/10.1186/1746-6148-9-139>, 139–139.
- Terry, R.S., Smith, J.E., Dunn, A.M., 1998. Impact of a novel, feminising microsporidium on its crustacean host. *J. Eukaryot. Microbiol.* 45, 497–501.
- Vey, A., Vago, C., 1973. Protozoan and fungal diseases of *Austropotamobius pallipes* Lereboullet in France. In: Abrahamsen, E.S. (Ed.), *Freshwater Crayfish*. Lund.
- Vivares, C.P., 1980. An ultrastructural study of *Thelohania maenadis* Perez (Microspora, Microsporidia) and new facts on the genus *Thelohania* Henneguy. *Arch. Protistenkd.* 123, 44–60.
- Vossbrinck, C.R., Debrunner-Vossbrinck, B.A., 2005. Molecular phylogeny of the Microsporidia: ecological, ultrastructural and taxonomic considerations. *Folia Parasitologica* 52, 131–142.
- Wang, T.-C., Nai, Y.-S., Wang, C.-Y., Solter, L.F., Hsu, H.-C., Wang, C.-H., Lo, C.-F., 2013. A new microsporidium, *Triwangia cardiniae* gen. nov., sp. nov. parasitizing fresh water shrimp, *Caridina formosa* (Decapoda: Atyidae) in Taiwan. *J. Invertebr. Pathol.* 112, 281–293. <http://dx.doi.org/10.1016/j.jip.2012.12.014>.
- Weiss, L.M., Zhu, X.L., Cali, A., Tanowitz, H.B., Wittner, M., 1994. Utility of microsporidian rRNA in diagnosis and phylogeny: a review. *Folia Parasitologica* 41, 81–90.
- Wittner, M., Weiss, L.M., 1999. The Microsporidia and Microsporidioses. American Society for Microbiology, Washington, DC, USA.